energies

MDPI

Article

A Hybrid LQR–PI Control Strategy with Virtual Impedance for Next-Generation Inverter-Based Microgrids: Enhanced Dynamic Stability and Power Quality

Douaoudi Said [1], Djilali Toumi [1], Emad Abd-Elrady [2,*], Mhamed Larbi [1], Sarra Adiche [1], Riyadh Bouddou [3], Ali Aillane [4] and Mohamed I. Mosaad [5]

[1] L2GEGI Laboratory, Department of Electrical Engineering, University of Tiaret, Tiaret 14000, Algeria; said.douaoudi.etd@univ-tiaret.dz (D.S.); djilali.toumi@univ-tiaret.dz (D.T.); mhamed.larbi@univ-tiaret.dz (M.L.); sarra.adiche@univ-tiaret.dz (S.A.)
[2] Faculty of Engineering Technology & Science, Higher Colleges of Technology, Abu Dhabi P.O. Box 25026, United Arab Emirates
[3] Department of Electrical Engineering, Faculty of Technology, University of Naama, Naama 45000, Algeria; bouddou@cuniv-naama.dz
[4] Laboratory of Applied Automation, Department of Automation and Electrification, Faculty of Hydrocarbons and Chemistry, M'Hamed Bougara University of Boumerdes, Boumerdes 35000, Algeria; a.aillane@univ-boumerdes.dz
[5] Yanbu Industrial College, Royal Commission Yanbu Colleges Institutes, Yanbu 46452, Saudi Arabia; m_i_mosaad@hotmail.com
* Correspondence: emad.abdelrady@hct.ac.ae

Abstract

Advanced control strategies for inverter-based distributed energy resources (DERs) are essential to ensure stable, reliable, and high-quality operation of modern islanded microgrids (MGs) as renewable energy penetration increases. This paper proposes a hybrid optimal control framework that combines a Linear Quadratic Regulator (LQR) with a Proportional–Integral (PI) controller and integrates droop control with a virtual impedance technique to improve the dynamic performance, power-sharing capability, and power quality of inverter-based MGs. The PI controller regulates the inverter current, while the LQR provides optimal state feedback to improve transient response and disturbance rejection. Primary droop control enables decentralized active and reactive power sharing, whereas secondary control restores voltage and frequency to their nominal values following load disturbances. Furthermore, the virtual impedance technique mitigates the adverse effects of line impedance mismatches and improves power-sharing accuracy among distributed generators. The proposed control strategy was validated through MATLAB/Simulink simulations that accounted for dynamic load variations. Compared with a conventional PI controller, the proposed hybrid LQR–PI approach reduced the frequency settling time from 0.5 s to 0.2 s, decreased the voltage recovery time from 0.5 s to 0.25 s, and achieved reduced voltage and current total harmonic distortion (THD) compared with the conventional PI control, despite the higher control energy. The optimal state feedback provided by the LQR contributed to improved transient performance, while the virtual impedance technique enhanced system robustness and maintained accurate power sharing under uncertain operating conditions. The obtained results demonstrate that the proposed control framework provides an effective and computationally efficient solution for next-generation inverter control in islanded MGs, offering enhanced dynamic stability, improved power quality, and reliable operation of renewable-energy-based distributed power systems.

Check for updates

Academic Editors: Nick Papanikolaou and Miao Yu

Received: 19 August 2026
Revised: 19 October 2026
Accepted: 22 October 2026
Published: 26 October 2026

Copyright: © 2026 by the authors. Licensee MDPI, Basel, Switzerland. This article is an open access article distributed under the terms and conditions of the Creative Commons Attribution (CC BY) license.

Keywords: hybrid LQR–PI control; inverter-based microgrids; virtual impedance; droop control; optimal control; distributed energy resources; dynamic stability; power quality; secondary control

1. Introduction

The rapid integration of renewable energy sources and distributed energy resources (DERs) into modern power systems has accelerated the transition toward decentralized, flexible, and intelligent energy infrastructures. However, the intermittent nature of renewable generation, the increasing penetration of power electronic converters, and the growing demand for high-quality electricity have introduced significant challenges in voltage regulation, frequency stability, transient performance, and power-sharing accuracy. In this context, microgrids (MGs) have emerged as a promising solution for integrating renewable-based generation units while enhancing grid resilience, reliability, and operational flexibility [1,2].

A microgrid is a localized energy system composed of multiple distributed generation (DG) units, such as photovoltaic (PV) systems, wind turbines, diesel generators, battery energy storage systems, and controllable loads, operating as a coordinated entity [3,4]. According to IEEE standards, MGs are capable of controlling DERs to provide reliable power under both grid-connected and islanded operating conditions. During grid-connected operation, the MG exchanges power with the utility network, whereas in islanded mode, inverter-based DG units must autonomously regulate voltage and frequency while ensuring appropriate active and reactive power (*Ps* and *Qs*) sharing among parallel converters [5–7]. Therefore, advanced inverter control strategies that maintain stable operation under dynamic and uncertain conditions have become a critical research direction for next-generation power electronic systems.

During islanded operation, maintaining stable voltage and frequency while ensuring accurate power sharing among distributed generation units remains a main challenge in inverter-based MGs. Seamless transitions between grid-connected and islanded modes requires advanced control strategies capable of maintaining system stability and minimizing transient deviations during operating mode changes. D'silva et al. [8] investigated the transition challenges between grid-connected and islanded MG operation and highlighted the importance of robust control mechanisms for achieving smooth mode transitions and reliable autonomous operation. Furthermore, Sun et al. [9] proposed an optimized autonomous control strategy for islanded systems to simultaneously regulate frequency, voltage, and power-sharing accuracy among distributed generators, thereby demonstrating the necessity of coordinated control approaches to improve MG stability. More recently, Nurunnabi et al. [10] analyzed advanced grid-forming inverter technologies and their PQ capabilities, emphasizing the critical role of inverter-based control frameworks in achieving enhanced voltage regulation and improved PQ in future decentralized energy systems.

The increasing deployment of MGs worldwide demonstrates their strategic importance in future energy systems. In the United States, hundreds of operational MGs with several gigawatts of installed capacity have been developed to improve grid resilience and provide backup power for critical infrastructures [11–13]. Similarly, India has actively promoted microgrid and mini-grid deployment, particularly in rural areas, through national renewable energy programs [14,15]. In Sub-Saharan Africa, countries such as Kenya and Nigeria have experienced significant growth in commercial and community MGs to improve energy access [16,17]. Europe and China have also accelerated MG development as part of their renewable energy expansion strategies and decarbonization

objectives [18–21]. These global developments highlight the necessity of robust inverter-based control approaches to support the reliable integration of renewable energy.

Modern MGs typically employ a hierarchical control structure comprising primary, secondary, and tertiary control layers, each addressing distinct operational objectives: stability, power quality (PQ), and energy management [22,23]. Among these layers, primary control plays a fundamental role in maintaining the autonomous operation of inverter-based DG units. In AC MGs, conventional droop control strategies based on $P-$frequency ($Ps-f$) and $Qs-$voltage ($Qs-V$) relationships enable decentralized power sharing between parallel inverters without communication requirements [24,25]. However, conventional droop controllers suffer from several limitations, including slow transient response, voltage and frequency deviations, and inaccurate power sharing caused by mismatched line impedances. To overcome these challenges, virtual impedance techniques have been widely investigated to improve power decoupling, enhance stability, and mitigate the effects of physical line impedance variations [26,27].

Secondary control is responsible for eliminating steady-state deviations introduced by primary control and restoring voltage and frequency to their nominal values after disturbances. Depending on communication requirements, secondary control can be implemented using centralized, distributed, or decentralized approaches [28]. This control layer becomes particularly important during islanding transitions and under dynamic loading conditions, where the rapid restoration of voltage and frequency is essential to maintaining power quality (PQ) and system reliability [29]. Meanwhile, tertiary control optimizes power exchange between the microgrid and external networks while improving economic operation and the utilization of renewable energy [30,31].

Despite significant advances in inverter-based MG control, achieving fast transient response and high-quality voltage regulation under uncertain operating conditions remains challenging. The performance of MG controllers strongly depends on the ability of power electronic converters to regulate the output voltage and frequency in accordance with grid requirements and IEEE standards [32]. Although droop control provides an effective decentralized solution, its dependence on network impedance characteristics limits its performance in practical systems. Therefore, virtual impedance has been introduced as an additional control mechanism to improve impedance matching and enhance power-sharing capability [33,34].

Furthermore, conventional proportional–integral (PI) controllers remain widely used in inverter control applications due to their simplicity and ease of implementation. However, PI-based strategies often exhibit limited disturbance rejection capability and slow dynamic response under severe load variations. Consequently, voltage and frequency deviations may persist for extended periods, reducing system robustness and affecting PQ [35–37]. Although several advanced control techniques have been proposed, many approaches introduce increased computational complexity, sensitivity to parameter variations, or implementation challenges, limiting their applicability in practical inverter-based systems. To address these limitations, this paper proposes an advanced hybrid Linear Quadratic Regulator–Proportional–Integral ($LQR-PI$) control strategy with virtual impedance for inverter-based islanded MGs. The proposed approach combines the optimal state-feedback capability of LQR control with the simplicity and steady-state accuracy of PI regulation while incorporating droop control and secondary restoration mechanisms to improve dynamic performance. The proposed framework aims to provide a robust and efficient solution for next-generation inverter control in renewable-based decentralized power systems.

The main objectives of this work are:

- To develop a hybrid $LQR - PI$ control framework for inverter-based DG units to improve voltage and frequency regulation under dynamic load variations.
- To integrate virtual impedance into the control structure to enhance active and reactive power-sharing performance under line impedance mismatches.
- To evaluate the effectiveness of the proposed controller compared with conventional PI-based control in terms of transient response, voltage recovery, frequency stabilization, and harmonic distortion.
- To demonstrate the capability of the proposed approach to support reliable and high-quality operation of islanded MGs with renewable energy integration.

The main contributions of this paper can be summarized as follows:

- A hybrid optimal control strategy, combining LQR and PI controllers, is developed for inverter-based MGs, providing improved transient response and disturbance rejection compared with conventional PI control.
- A coordinated control framework integrating droop control, virtual impedance, and secondary regulation is proposed to enhance voltage/frequency restoration and power-sharing accuracy.
- A comprehensive MATLAB/Simulink evaluation is conducted under dynamic load disturbances, demonstrating reductions of 60% in frequency stabilization time (from 0.5 s to 0.2 s), 50% in voltage recovery time (from 0.5 s to 0.25 s), and reduced voltage and current THD compared with the conventional PI control.

The proposed strategy provides a practical pathway toward advanced inverter control for decentralized renewable-energy-based MGs.

The remainder of this paper is organized as follows. Section 2 presents a review of existing inverter-based MG control strategies and discusses their limitations. Section 3 describes the proposed methodology, including droop control, virtual impedance implementation, secondary voltage and frequency restoration, inner control loops, mathematical modeling, and LQR controller design. Section 4 presents the simulation results and a comparative analysis between the proposed $LQR - PI$ approach and conventional PI control. Finally, Section 5 concludes the paper and discusses future research directions.

2. Related Works

The increasing penetration of inverter-based DERs has motivated the development of advanced control strategies for power electronic converters operating in MG environments. Next-generation inverter control requires improved capabilities in dynamic stability, voltage and frequency regulation, harmonic mitigation, and robustness to nonlinear and rapidly varying operating conditions. Several control approaches have been investigated, including advanced feedback techniques, virtual synchronous machine concepts, optimization-based methods, predictive control, and artificial intelligence (AI)-based strategies. However, achieving an effective balance between dynamic performance, computational efficiency, and practical implementation remains a major challenge.

Early studies focused on improving PQ and harmonic attenuation in inverter-dominated systems. A harmonic reduction approach for standalone PV-based MGs was proposed using filtering techniques to mitigate load-side disturbances and improve waveform quality. Although effective under specific operating conditions, the proposed method lacked adaptability when subjected to significant variations in load characteristics and system dynamics [38]. In another study, droop control, Virtual Synchronous Machine (VSM), and Virtual Oscillator Control (VOC) strategies were compared for islanded parallel inverters. These approaches improved synchronization capability and power-sharing performance; however, their effectiveness in maintaining PQ during fast transient events remained limited [39].

Optimization-based control techniques have also received considerable attention for improving the operation of inverter-based energy systems. A Hybrid Lion–Crow Search Algorithm was employed for the optimal placement and sizing of Unified PQ Conditioner (UPQC) devices to reduce power losses and harmonic distortion in distribution networks. Nevertheless, reliance on offline optimization and static operating assumptions limits its applicability in highly dynamic real-time environments [40]. Similarly, a self-tunable controller combined with a switched-capacitor inverter for fuel-cell-based MGs demonstrated improved energy regulation performance, although the increased controller complexity presents challenges for practical implementation and scalability [41].

Predictive and model-based control strategies have been extensively investigated due to their ability to provide fast and accurate converter regulation. Advanced voltage control schemes for interlinking converters have improved predictive performance; however, their implementation requires significant computational resources, which may limit their application in large-scale, resource-constrained inverter systems [42]. Furthermore, active damping techniques based on grid-side current feedback have been proposed for LCL-filtered converter systems to suppress harmonic oscillations. Despite their effectiveness, these approaches were primarily developed for grid-connected applications and may require further adaptation for isolated MGs containing multiple distributed generators [43].

Recently, intelligent and metaheuristics-based control approaches have emerged as promising solutions for handling uncertainties and nonlinearities in renewable-energy-based systems. Atom Search Optimization (ASO) was applied to control hybrid PV–wind–battery systems and improve voltage and current quality. However, the associated tuning complexity and response latency may affect real-time implementation capability [44]. Artificial Neural Network (ANN)-based controllers have also been investigated for adaptive load regulation in islanded MGs, thereby providing improved adaptability to nonlinear systems. Nevertheless, their dependence on training data, computational requirements, and implementation complexity remain important limitations [45].

Other optimization and intelligent control methods have been developed for PQ enhancement applications. The Sine Cosine Search Optimization (SCSO) algorithm was applied to UPQC systems to improve harmonic compensation performance. Although improved suppression capability was achieved, the method requires careful parameter adjustment and may exhibit reduced robustness under highly variable operating conditions [46,47]. Similarly, a Modulated-UPQC integrated with switched-inductor boost converters was proposed for hybrid AC/DC MGs using optimization-based control techniques. Despite achieving improved PQ regulation, the resulting control structure remains complex for real-time deployment in practical systems [48].

Model Predictive Control (MPC) has also been widely studied for inverter-based energy management and converter control due to its high accuracy and ability to handle multiple constraints. However, MPC requires accurate mathematical models and significant computational resources, which can limit its suitability for highly dynamic systems and embedded implementations [49]. Furthermore, fuzzy-based space vector pulse width modulation (FSV-PWM) control strategies have been proposed for inverter clusters, achieving acceptable harmonic performance under uncertainty. Nevertheless, maintaining consistent performance under wide variations in operating states remains challenging [50].

Despite these significant developments, existing control approaches still face several limitations, including high computational burden, complex parameter tuning, limited scalability, and insufficient transient performance under severe disturbances. Therefore, there remains a need for advanced yet practical inverter control strategies that can combine fast dynamic response, robust disturbance rejection, and improved PQ without excessive

computational requirements. To provide a comprehensive assessment of existing advanced control approaches and clearly identify the research gap addressed in this study, a comparative analysis of representative inverter-based MG control strategies and the proposed $LQR - PI$ framework is presented in Table 1. The reviewed approaches include nonlinear controllers, intelligent control techniques, optimization-based methods, observer-based strategies, and advanced PID-based schemes. Although these methods have demonstrated significant improvements in voltage regulation, disturbance rejection, PQ enhancement, and system robustness, several limitations remain, including high computational requirements, complex parameter tuning procedures, dependence on accurate system models, limited scalability, and challenges associated with practical real-time implementation. Therefore, a control strategy that balances dynamic performance, robustness, implementation simplicity, and applicability across inverter-based microgrid configurations remains required. The proposed $LQR - PI$ control approach is positioned within this context by combining optimal state feedback, conventional PI regulation, droop control, and virtual impedance to enhance transient stability and PQ while maintaining a practical and scalable control structure.

Although significant efforts have been devoted to improving inverter-based MG performance using nonlinear, intelligent, and optimization-based control strategies, most existing approaches suffer from increased computational complexity, extensive parameter tuning requirements, limited scalability, or challenges related to real-time implementation. Therefore, there is still a need for a control strategy that provides an effective balance between dynamic performance, robustness, implementation simplicity, and applicability to practical inverter-based systems.

To address these challenges, this paper proposes a hybrid LQR–PI control framework integrated with droop control, virtual impedance, and secondary regulation for inverter-based MGs. Unlike highly complex optimization and AI-based controllers, the proposed approach combines the advantages of optimal state feedback and conventional PI regulation to achieve improved transient stability, faster voltage/frequency restoration, and enhanced harmonic performance while maintaining implementation simplicity. This makes the proposed strategy suitable for next-generation inverter control applications in decentralized renewable energy systems.

Table 1. Comparative analysis of existing advanced control strategies and the proposed LQR–PI framework.

Ref.	Control Strategy	Studied System	Control Complexity	Computational/ Implementation Cost	Main Advantages and Contributions	Main Limitations	Transferability to Other Systems	Comparison with Proposed LQR–PI Control Strategy
[51]	Robust integral backstepping control combined with DPC and SVM	Grid-connected PV MG with PV/BESS through multifunctional VSI	High. Backstepping requires recursive nonlinear control design and accurate system modeling	High due to nonlinear computation and DPC-SVM implementation requirements	Provides robust power regulation, improved tracking performance, and disturbance rejection for PV/BESS systems	High controller complexity and dependency on system parameters limit practical implementation	Moderate. Applicable to renewable inverter systems but requires redesign for different converter structures	The proposed LQR–PI provides a simpler optimal control structure while achieving improved transient response and PQ with lower implementation complexity
[52]	Adaptive Fuzzy Logic Control (FLC)	Hybrid PV/wind MG connected system	Medium–high. Requires fuzzy rule design and adaptive mechanisms	Moderate–high due to online adaptation and fuzzy inference operations	Improves robustness against renewable generation variations and nonlinear operating conditions	Performance depends on membership functions and tuning process; scalability may be challenging	High for renewable systems with uncertainty, but requires fuzzy redesign	Compared with adaptive FLC, the proposed LQR–PI avoids complex rule tuning while maintaining fast voltage/frequency regulation through optimal feedback
[53]	NARX-RBF Neural Network intelligent control	Hybrid energy storage system for MG energy management	Very high. Requires neural network training and optimization	High due to training requirements and computational burden	Provides intelligent prediction capability and improved energy management under variable conditions	Requires large training datasets, offline training, and may suffer from generalization issues	Limited without retraining for different systems and operating conditions	The proposed approach offers lower computational cost and easier deployment while providing robust inverter-level control without training requirements
[54]	Synergetic control with simplified Super-Twisting Algorithm (STA)	PV/BESS-based DC MG	High. Based on nonlinear sliding-mode concepts and synergetic control theory	Medium–high due to nonlinear control calculations	Provides strong robustness against disturbances and improves DC MG stability	Requires accurate parameter selection; possible chattering and implementation complexity	Moderate. Mainly suitable for DC MG applications	The proposed LQR–PI approach provides simpler implementation and focuses on AC inverter regulation with improved transient performance
[55]	Genetic Algorithm optimized Type-2 FLC with Fractional-Order Technique	Microgrid system under uncertain operating conditions	Very high. Combines evolutionary optimization, type-2 FLC, and fractional-order control	Very high due to optimization process and fuzzy computation	Achieves high robustness and improved control under uncertainty	Large computational requirements and complex parameter tuning reduce real-time feasibility	Limited because optimization parameters must be recalculated for new systems	The proposed LQR–PI offers a more practical compromise between performance and complexity while avoiding optimization-based tuning
[56]	Decentralized Active Fault-Tolerant Control using PI Unknown Input Observer	DC microgrid with actuator and source disturbances	High. Includes observer-based fault estimation and fault-tolerant control	Medium–high due to observer design and additional estimation algorithms	Enhances reliability under component faults and external disturbances	Mainly focused on fault tolerance rather than overall inverter performance and PQ	Moderate. Requires adaptation for different fault scenarios and converter topologies	The proposed strategy focuses on normal operating stability and power quality enhancement with a simpler architecture
[57]	Enhanced grid current and DC voltage regulation using advanced control under uncertainty	Three-level four-leg rectifier DC microgrid	High. Advanced converter control with uncertainty compensation	High due to converter complexity and multi-variable regulation	Improves DC voltage regulation and current quality under disturbances	Limited mainly to three-level rectifier-based DC systems; higher hardware complexity	Moderate due to dependence on converter topology	The proposed LQR–PI is more general for inverter-based microgrids and requires fewer hardware-specific modifications
[58]	Robust Type-2 FLC with DPC	PV microgrid with battery energy storage system through multifunctional VSI	High. Type-2 fuzzy inference combined with DPC	Medium–high due to fuzzy processing and tuning requirements	Provides robust operation under renewable fluctuations and improves PQ	Requires expert knowledge for fuzzy design and parameter adjustment	Moderate–high for renewable inverter applications	The proposed method achieves similar objectives using optimal control with lower tuning complexity and easier practical implementation
[59]	Multi-stage PID controller based on CDM	Isolated MG with electric vehicle aggregation	Medium. Advanced PID tuning using CDM methodology	Low–medium compared with intelligent methods	Improves frequency regulation and dynamic response under different operating conditions	Mainly focused on frequency control; limited voltage regulation and power quality analysis	High due to PID-based structure	The proposed LQR–PI provides simultaneous voltage/frequency regulation, virtual impedance-based power sharing, and THD improvement

3. Methodology and Modeling

3.1. Droop Control Strategy for DG in MGs

The DG units employ droop control to regulate both the amplitude and frequency of their AC output voltage [60]. In configurations involving parallel inverters, droop control facilitates equitable load sharing among the inverters, with its effectiveness influenced by the impedance characteristics of each DG unit relative to the AC bus [61]. To enable the implementation of $Ps - f$ and $Qs - V$ droop control, an additional virtual impedance is introduced alongside the existing physical impedance. This approach enhances the decoupling of Ps and Qs flows and mitigates the adverse effects of mismatched line impedances [62]. The adoption of this technique in the present study aims to significantly improve the dynamic and steady-state performance of the system under investigation. The simplified structure of the equivalent circuit of an MG in islanding mode is shown in Figure 1. The voltage source inverter (VSI) is connected to the point of common coupling (PCC) through the line impedance Z_L. $E\angle\delta$ is the output voltage of the VSI, $V\angle 0$ is the PCC voltage, wherein power angle δ is the phase angle between the PCC voltage and the output voltage inverter, Z_L is line impedance, X_L is the output reactance of the inverter [22].

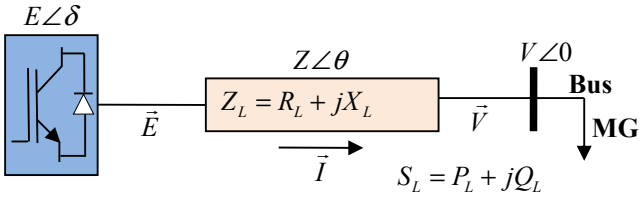


Figure 1. Equivalent circuit of an MG in islanding mode.

The Ps and Qs delivered from the DG unit to terminal V is described in Equations (1) and (2).

$$P_L = \left(\frac{EV}{Z_L}\cos\delta - \frac{V^2}{Z_L}\right)\cos\theta + \frac{EV}{Z_L}\sin\delta\sin\theta \tag{1}$$

$$Q_L = \left(\frac{EV}{Z_L}\cos\delta - \frac{V^2}{Z_L}\right)\sin\theta - \frac{EV}{Z_L}\sin\delta\cos\theta \tag{2}$$

where E and V are the amplitudes of the inverter output voltage and the PCC voltage, respectively, while δ represents the power angle. The analysis considers only inductive line impedance, corresponding to a power factor angle of $\theta = 90°$. Additionally, the inverter's Ps and Qs is expressed in terms of current and voltage components in the synchronous reference frame, as given in Equation (3).

$$\begin{cases} P_L = \frac{3}{2}\left(V_{fd}\cdot i_{od} + V_{fq}\cdot i_{oq}\right) \\ Q_L = \frac{3}{2}\left(-V_{fd}\cdot i_{oq} + V_{fq}\cdot i_{od}\right) \end{cases} \tag{3}$$

In cases where the power angle δ is small (less than 0.1 rad), it is reasonable to approximate $sin\delta \approx \delta$ and $cos\delta \approx 1$. By applying these approximations to the simplified forms of Equations (1) and (2), the partial derivatives of the Ps and Qs, P_L and Q_L can be derived as presented in Equation (4).

$$\begin{cases} \frac{\partial P_L}{\partial E} = \frac{V}{X_L}\delta \\ \frac{\partial P_L}{\partial \delta} = \frac{EV}{X_L} \end{cases} \& \begin{cases} \frac{\partial Q_L}{\partial E} = \frac{V}{X_L} \\ \frac{\partial Q_L}{\partial \delta} = 0 \end{cases} \tag{4}$$

According to Equation (4), the power angle δ has the greatest influence on the Ps injected from the inverter into the common bus. In contrast, the amplitude difference

between E and V significantly affects Qs. Moreover, by adjusting the inverter's output-voltage frequency, the inverter's phase can be modified [63,64]. Consequently, the inverter's output power is primarily regulated through wireless control of parallel-connected inverters using frequency droop for Ps and voltage droop for Qs The corresponding droop control characteristics for Ps and Qs are expressed by the $Ps - f$ and $Qs - V$ equations, respectively, as follows:

$$f = f_n^* - m_P(P - P^*) \tag{5}$$

$$E = E_n^* - n_q(Q - Q^*) \tag{6}$$

where m_p, n_p, P^*, and Q^* stand for the frequency droop coefficient, voltage droop coefficient, real Ps output, and real Qs output, respectively. In addition, the rated frequency is represented by f_n^*, and the rated voltage amplitude by E_n^*. Equations (7) and (8) represent frequency and voltage droop coefficients.

$$m_p = \frac{\Delta f}{P_{\max}} \tag{7}$$

$$n_q = \frac{\Delta E}{2Q_{\max}} \tag{8}$$

where the maximum permitted variations in voltage and frequency are denoted by ΔE and Δf, respectively. The system's nominal Ps and Qs supplies are denoted by P_{max} and $Q_{\max}$ respectively [65]. Moreover, the droop characteristics given by Equations (7) and (8) are shown in Figure 2.

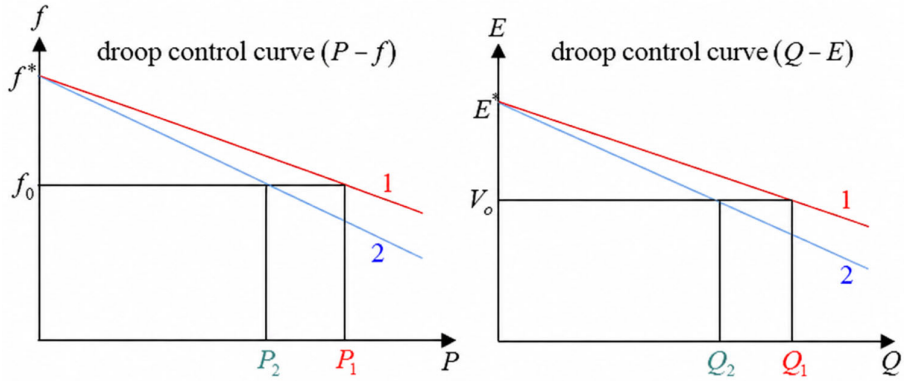


Figure 2. Conventional droop characteristics for an AC MG with inductive impedance [66].

3.2. Implementation and Role of Virtual Impedance in MG Control

To ensure a predominantly inductive behavior in the distribution line, a virtual impedance is introduced in addition to the existing physical line impedance. This modification helps establish a clear decoupling between Ps and Qs control, where Ps is primarily governed by the power angle, and Qs is controlled by the voltage magnitude [66]. This setup is essential for the effective implementation of P-f and Q-V droop control. The selection of this droop control method is motivated by the fact that most modern electrical loads are inductive [67]. The virtual impedance is embedded within the inverter's control system, specifically within the current feedback loop, to dynamically influence the voltage reference as depicted in Figure 3 [68]. In the synchronous rotating reference frame (dq frame), the virtual impedance can be mathematically modeled as follows:

$$\begin{cases} v_{fd}^* = E_d + \omega L_v i_{oq} - R_v i_{od} \\ v_{fq}^* = E_q - \omega L_v i_{od} - R_v i_{oq} \end{cases} \tag{9}$$

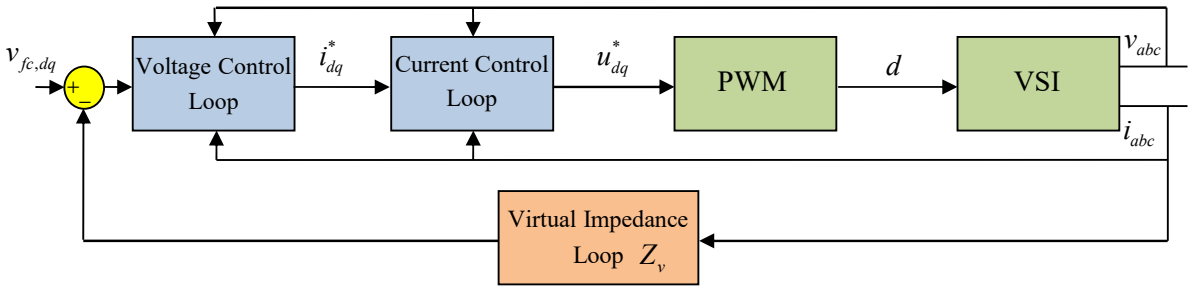


Figure 3. Implementation of virtual impedance control.

3.3. Voltage and Frequency Restoration via Secondary Control in Isolated MGs

To improve the quality of the power supply in MG and the accuracy of voltage distribution, secondary-level control of MG should be adopted to adjust the frequency and voltage amplitude setpoints. One of the most important properties of secondary control is that it must operate sufficiently slower than droop control to avoid interference between them. Different objectives, including economic optimization, voltage profile optimization, and overall loss reduction, can be targeted through secondary control in the MG [69].

After this brief introduction, the equations of the frequency value and inverter output voltage of f and E are expressed as follows:

$$\begin{cases} f = f_n^* + m_q(Q - Q^*) + f_S \\ E = E_n^* - n_p(P - P^*) + E_S \end{cases} \tag{10}$$

With:

$$\begin{cases} f_S = \left(k_{pf} + \frac{k_{if}}{s}\right)(f_n^* - f) \\ E_S = \left(k_{pv} + \frac{k_{iv}}{s}\right)(E_n^* - E) \end{cases} \tag{11}$$

where k_{pf} and k_{if} represent the proportional and integral coefficients of the frequency regulator, k_{pv} and k_{iv} represent the coefficients for the proportional and integral voltage controller, f_n^* and E_n^*, are the nominal values of the frequency and voltage reference, and f_s and E_s, represent the frequency and voltage of the secondary control output, respectively. The functional control diagram of the primary control (droop control) and secondary control is shown in Figure 4.

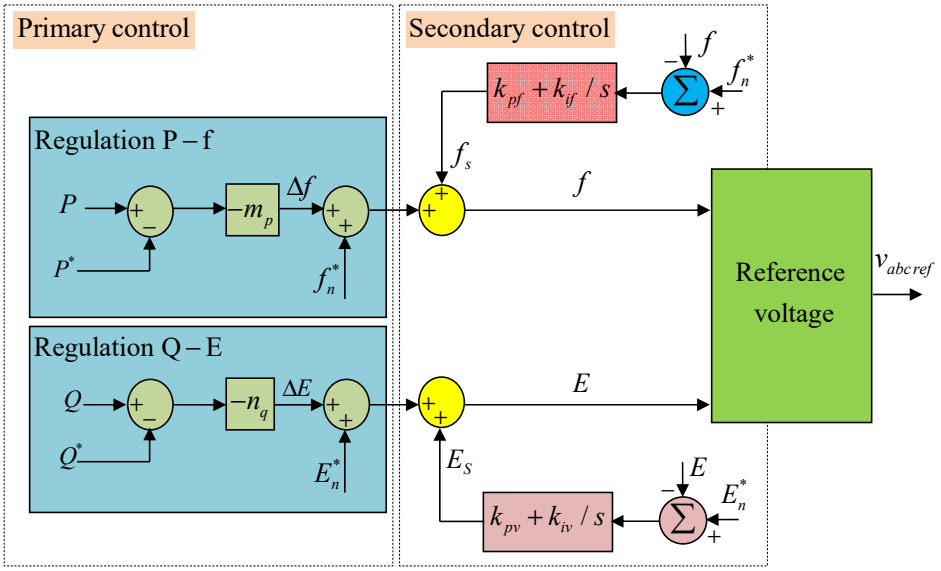


Figure 4. The functional control diagram of primary associated with secondary control.

3.4. Inner Current and Voltage Control Loops

The goal of any control system is to track the system's response to reference data and maintain system stability in a closed loop. This control structure has an external voltage loop that provides the current reference and an internal current loop that provides the modulation signals for the inverter. It is often chosen to control the current and/or the output voltage of the *VSI* in *MGs*, this control level is detailed in [70,71]. Figure 5 presents a diagram illustrating the control of an islanding *MG* with an *LC* filter.

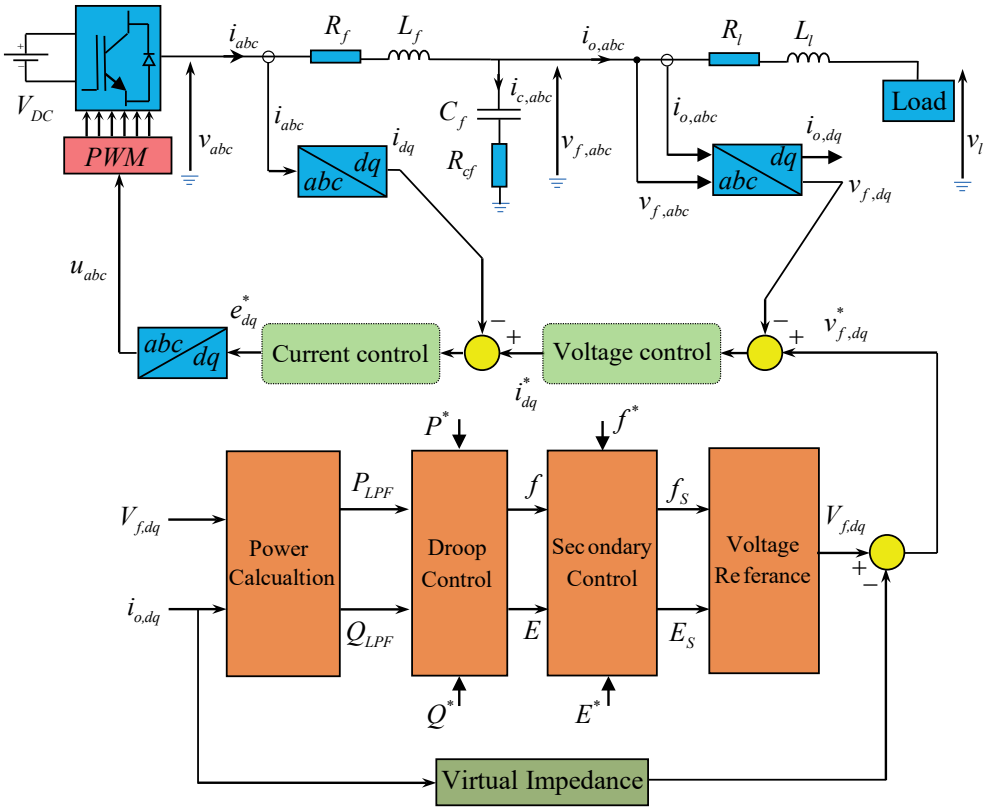


Figure 5. Control system of islanded MG with LC filter.

In Figure 5, L_f is the filter inductor and R_f is the equivalent series resistance of the inductor filter; C_f is the filter capacitor and R_{cf} is the equivalent series resistance of the capacitor filter; L_l is the load side line inductance; R_l is the equivalent series resistance of the line-side load; i_{abc} is the inductor current, v_{fabc} is the capacitor voltage, and i_{oabc} is the output current of the *DG* unit.

3.5. Mathematical Model of the System

By applying Kirchhoff's law of current (*KCL*) and voltage (*KVL*) and the application of Park transformation to the equations of the system in the real reference frame, the following equations are obtained:

The *dq* components of the voltage across the capacitor filter:

$$\begin{cases} v_d = L_f s i_d + R_f i_d + v_{fd} - \omega L_f i_q \\ v_q = L_f s i_q + R_f i_q + v_{fq} + \omega L_f i_d \end{cases} \tag{12}$$

The equation of the inverter output current:

$$\begin{cases} i_d = i_{cd} + i_{od} \\ i_q = i_{cq} + i_{oq} \end{cases} \tag{13}$$

The dq components of the current in the capacitor:

$$\begin{cases} i_{cd} = C_f s v_{fd} - \omega C_f v_{fq} \\ i_{cq} = C_f s v_{fq} + \omega C_f v_{fd} \end{cases} \tag{14}$$

$$\begin{cases} v_{fd} = R_l s i_{od} + L_l s i_{od} + v_{ld} - \omega L_l i_{oq} \\ v_{fq} = R_l s i_{oq} + L_l s i_{oq} + v_{lq} + \omega L_l i_{od} \end{cases} \tag{15}$$

Substituting (15) into (13), and after rearrangement, the following equations are obtained:

$$\begin{cases} i_d = C_f s v_{fd} - \omega C_f v_{fq} + i_{od} \\ i_q = C_f s v_{fq} + \omega C_f v_{fd} + i_{oq} \end{cases} \tag{16}$$

A. Current controller

The inner current control is developed by standard feedback control. It commonly uses a PI controller (Figure 6). Thus, the current control can be expressed as

$$\begin{aligned} e_d^* &= (i_d^* - i_d)(K_{pi} + K_{ii}/s) - \omega L_f i_q + v_{fd} \\ e_q^* &= (i_q^* - i_q)(K_{pi} + K_{ii}/s) + \omega L_f i_d + v_{fq} \end{aligned} \tag{17}$$

where e_d^* and e_q^* are dq modulating signal components of the inverter, i_d and i_q are the inductor current values of dq axis components, v_{fd} and v_{fq} are the output filter voltage components, and ω is the frequency of MG.

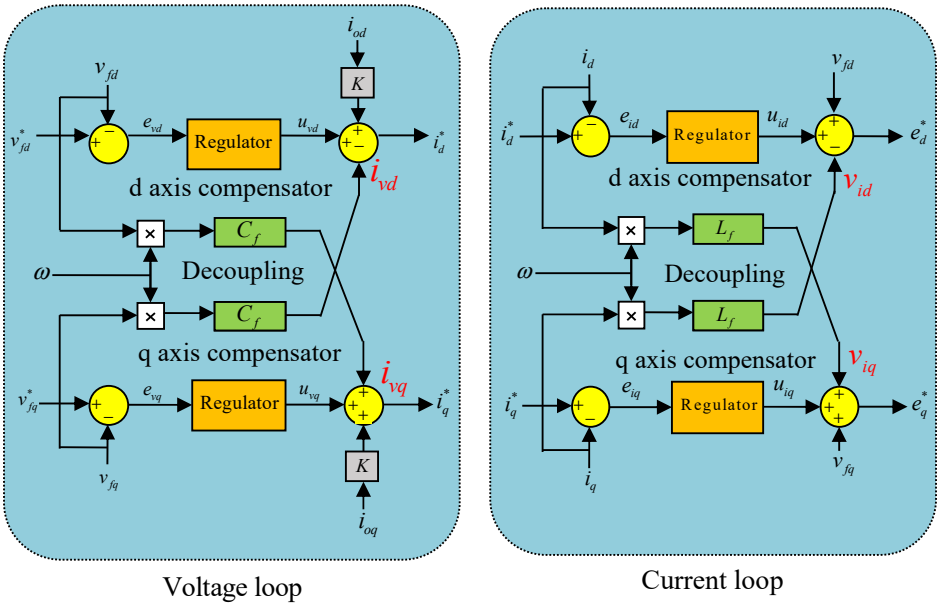


Figure 6. The comprehensive schematic of the two cascade loops.

B. Voltage controller

The outer voltage control is developed by using standard feedback/feedforward control and commonly uses a PI controller (Figure 6). Thus, the voltage control can be expressed as follows.

$$\begin{aligned} i_d^* &= (v_{fd}^* - v_{fd})(K_{pv} + K_{iv}/s) - \omega C_f v_{fq} + K i_{0d} \\ i_q^* &= (v_{fq}^* - v_{fq})(K_{pv} + K_{iv}/s) + \omega C_f v_{fd} + K i_{0q} \end{aligned} \tag{18}$$

where K is the current feedforward gain.

3.6. PI Controller Synthesis

PI Controllers of the current and voltage loops are synthesized by pole placement (ξ damping coefficients, ω_n natural frequency). The gain obtained coefficients are given by:

$$\begin{cases} K_{Pi} = 2\xi_i \omega_{ni} L_f - R_f \\ K_{ii} = \omega_{ni}^2 L_f \end{cases} \tag{19}$$

$$\begin{cases} K_{Pv} = 2\xi_v \omega_{nv} C_f \\ K_{iv} = \omega_{nv}^2 C_f \end{cases} \tag{20}$$

3.7. Design and Implementation of LQR Optimal Control

LQR is an optimal control that generates a steady state with minimal error and has strong control properties [72]. An important advantage of using an LQR strategy is that the system becomes asymptotically stable in the steady-state condition [73]. The principle of the control is to synthesize a vector K, which contains the gains associated with each state variable. It will be calculated using the quadratic linear control algorithm, which minimizes a quadratic criterion [74]. Integral action has been incorporated into the controller to eliminate steady-state errors [75]. To implement the proposed control, the classical *PI* In the voltage loop, LQR control is used, so the state space representation of the external voltage loop is required.

The state space representation is given as:

$$\begin{cases} \dot{X} = AX + BU \\ Y = CX + DU \end{cases} \tag{21}$$

From Equation (20) and Equation (16), the state space representation of the external voltage loop can be expressed as [76]:

$$\overbrace{\begin{bmatrix} \dot{v}_{fd} \\ \dot{v}_{fq} \end{bmatrix}}^{\dot{x}} = \overbrace{\begin{bmatrix} 0 & -\omega \\ \omega & 0 \end{bmatrix}}^{A} \overbrace{\begin{bmatrix} v_{fd} \\ v_{fq} \end{bmatrix}}^{x} + \overbrace{\frac{1}{C_f} I_{2x2}}^{B} \overbrace{\begin{bmatrix} i_{fd} \\ i_{fq} \end{bmatrix}}^{U} - \overbrace{\frac{1}{C_f} I_{2x2}}^{E} \overbrace{\begin{bmatrix} i_{od} \\ i_{oq} \end{bmatrix}}^{V} \tag{22}$$

where v_{fd} and v_{fq} are the two state vectors.

When the v_{fdq} voltage components are controlled, the output vector is given by:

$$Y = \overbrace{\begin{bmatrix} 1 & 0 \\ 0 & 1 \end{bmatrix}}^{C} \overbrace{\begin{bmatrix} v_{fd} \\ v_{fq} \end{bmatrix}}^{X} \tag{23}$$

To eliminate steady-state errors and ensure accurate tracking, an integral action is added to the control loop. The error vector between the reference voltage v_{fdq}^* and the measured output voltage $Y = v_{fdq}$ is defined as:

$$\dot{x}_e = v_{fdq}^* - Y = v_{fdq}^* - C \cdot x \tag{24}$$

By combining the original system state-space representation (Equation 21) with the error integrator dynamics, the augmented state-space model of the v_{fdq} voltage loop is formulated as:

$$\overbrace{\begin{bmatrix} \dot{x} \\ \dot{x}_e \end{bmatrix}}^{\dot{x}_g} = \overbrace{\begin{bmatrix} A & 0 \\ -C & 0 \end{bmatrix}}^{A_g} \overbrace{\begin{bmatrix} x \\ x_e \end{bmatrix}}^{x_g} + \overbrace{\begin{bmatrix} B \\ 0 \end{bmatrix}}^{B_g} U + \overbrace{\begin{bmatrix} E \\ 0 \end{bmatrix}}^{E_g} V + \begin{bmatrix} 0 \\ I \end{bmatrix} v_{fdq}^* \tag{25}$$

The output equation is given by:

$$Y = \overbrace{\begin{bmatrix} C & 0 \end{bmatrix}}^{C_g} x_g \tag{26}$$

where the augmented state vector becomes $x_g = \begin{bmatrix} v_{fd} & v_{fq} & \int\left(v_{fd}^* - v_{fd}\right) & \int\left(v_{fq}^* - v_{fq}\right) \end{bmatrix}^T$, used to compute $K_g = \begin{bmatrix} K & G \end{bmatrix}$ the optimal gain matrix of LQR controller, including integral action, as shown in Figure 7.

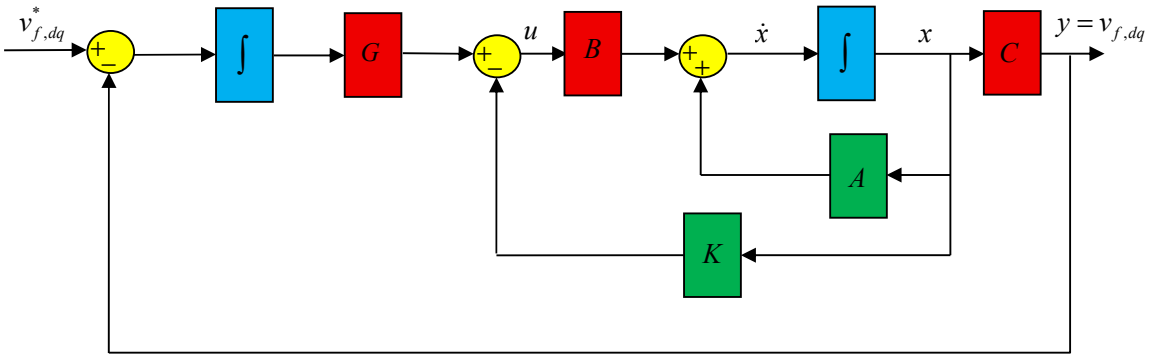


Figure 7. Block diagram of LQR.

Moreover, the simplified optimal control problem consists of finding the corrector matrix K_g, which minimizes the following cost function J:

$$J = \int_{t_o}^{t_f} \left(x_g^T(t)Q(t)x_g(t) + u^T(t)R(t)u(t)\right)dt \tag{27}$$

where Q and R represent the weighting matrices, and they are positive definite and symmetric. In our case, we chose $Q = {C_g}^T C_g$ and $R' > 100$, where $R' = 850$ and $R = R' I_{2x2}$.

Furthermore, if the pair $(A_g,\ B_g)$ is controllable and the pair $(A_g,\ C_g)$ is observable, then the following Riccati algebraic equation presents a unique positive definite symmetric matrix solution.

$$A_g^T P + PA_g + \rho Q - PB_g R^T B_g^T P = 0 \tag{28}$$

where P is the solution matrix of the Riccati equation (definite positive and symmetric) and ρ is the weight gain. We chose $\rho = 0.2$.

So, the state return matrix that minimizes J, defined in Equation (27), is given by [77]:

$$\begin{cases} U = -K_g x_g \\ K_g = R^{-1} B_g^T P \end{cases} \tag{29}$$

Design of the proposed LQR regulators:
Define system parameters ω and C_f;
Define the state space matrices $A_g,\ B_g$ and C_g;
Check eigenvalues and controllability of the system;
Define the weighting matrices Q and R.
where Q is multiplied by a scalar ρ to accelerate or decelerate the system, and then R' is multiplied by another scalar to impact how aggressively the controller acts.

With K_g representing the gain matrix that minimizes the cost function, x_g represents the solution to the continuous-time algebraic Riccati equation, which helps derive the

optimal controller, and P represents the closed-loop poles, which indicate the desired dynamics of the system when feedback is applied [78].

The proposed block diagram of the LQR regulator is given in Figure 7.

4. Simulation Results

To verify the effectiveness of the above-described control strategy based on the LQR method, this study used the MATLAB/Simulink 2024a environment to build the simulation model of an islanded MG with a fixed sampling time $T_s = 10^{-5}$s and $Ode1$ $(Euler)$ solver as a calculation method. Additionally, the system operated at a rated voltage of 230 V and a rated frequency of 50 Hz. The total power demand was 20 kW and 7 kVAR. In all the following scenarios, droop control with virtual impedance was used in the simulation. In this study, the allowable voltage variation was less than 5% (i.e., 15 V), and the acceptable frequency variation was typically less than 1.4% (i.e., 0.7 Hz), in accordance with the relevant standards. The transmission lines and distributed controllers are characterized in the following tables. Table A1 presents the parameters of the power stage and the controller; it is provided in Appendix A.

4.1. Study Scenarios

4.1.1. Scenario 1: PI Regulator's Response Without Secondary Control

Figures 8–11 illustrate the system frequency, output voltage, Qs, Ps, and both the direct and quadrature components of the inverter output voltage.

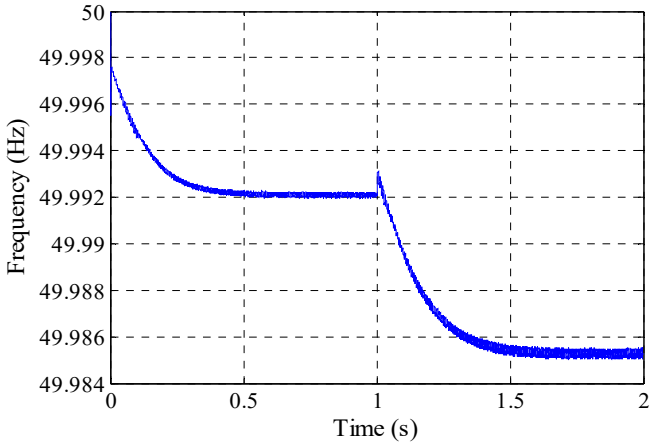


Figure 8. The frequency response of the PI regulator without secondary control.

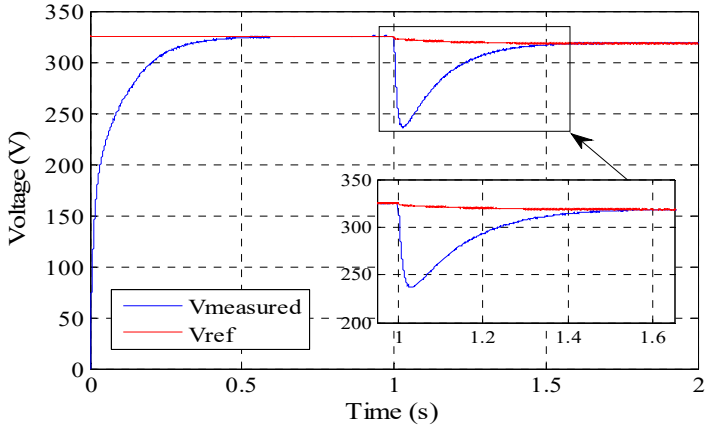


Figure 9. The voltage response of the PI regulator without secondary control.

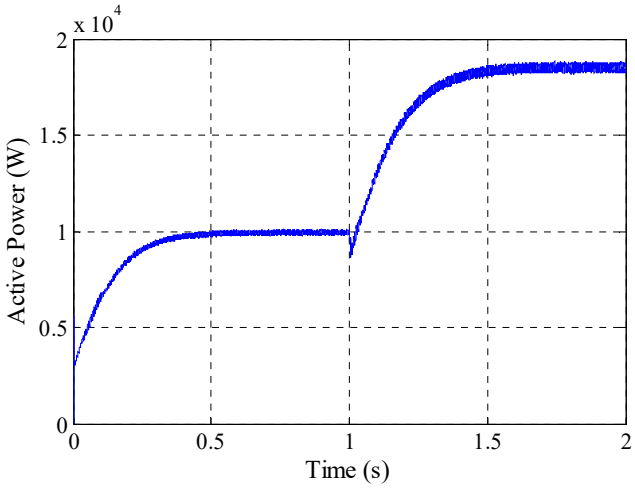


Figure 10. Active power response of the PI regulator without secondary control.

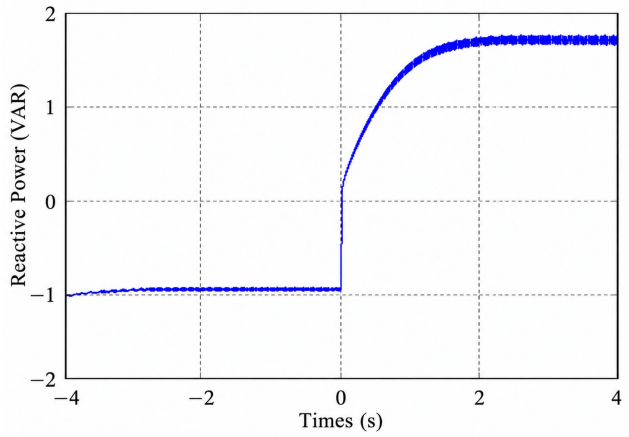


Figure 11. Reactive power response of the PI regulator without secondary control.

The simulation sequence was as follows: Until 1 s, the initial load demand was constant at $P_{load} = 10$ kW and $Q_{load} = 0$ kVAR. As a result, a decrease in frequency occurred with an increase in P. At 2 s, there was an increase in the load of $P_{load} = 10$ kW and $Q_{load} = 7$ kVAR, which led to an increase in the frequency drop to about 49.985 Hz and a drop in the output voltage amplitude to about 318 V. These results are consistent with the theory of $(Ps - f/Qs - V)$ droop control, and these values are within the standards mentioned previously. However, the frequency and output voltage took about 0.5 s to reach their final values. Additionally, this delay is clearly visible in the direct and quadrature voltage, due to the slow response of the PI regulator.

4.1.2. Scenario 2: Response of $LQR - PI$ Regulator Without Secondary Control

As in Scenario 1, the $Ps - f/Qs - V$ droop control strategies were effectively applied, keeping frequency and output voltage deviations within the acceptable limits. However, the results illustrated in Figures 12–17 demonstrate the superior dynamic performance of the proposed $LQR - PI$-based control scheme compared with the conventional PI regulator. When the additional load was applied at 2 s, the system exhibited a rapid and robust response, with minimal delay in both frequency and voltage stabilization. This enhanced responsiveness is particularly evident in the direct (d-axis) and quadrature (q-axis) voltage components, which recovered much more quickly than in Scenario 1. The improved performance is attributed to the optimal state feedback provided by the LQR, which enhanced the transient response and damping characteristics of the system. Nevertheless, it is important to note that secondary control remained necessary in both scenarios to fully

restore the DG unit's voltage and frequency to their nominal values after disturbances. The $LQR - PI$ regulator significantly improved the primary control response, but long-term stability and setpoint restoration required a coordinated secondary control strategy.

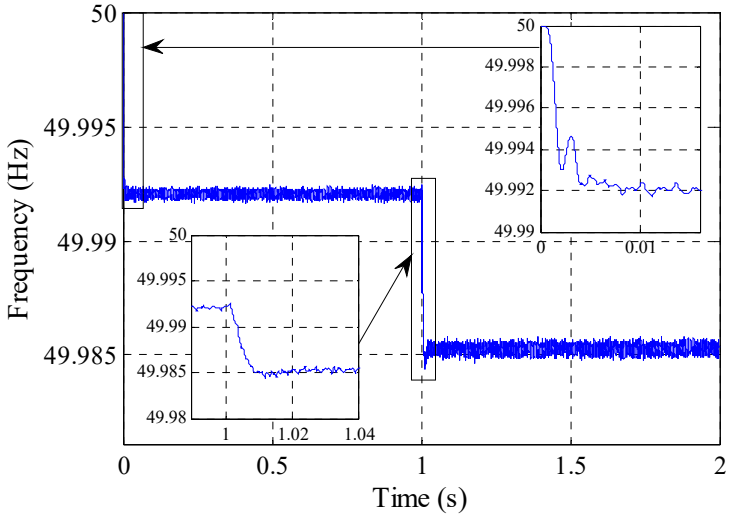


Figure 12. The frequency response of the $LQR - PI$ regulator without secondary control.

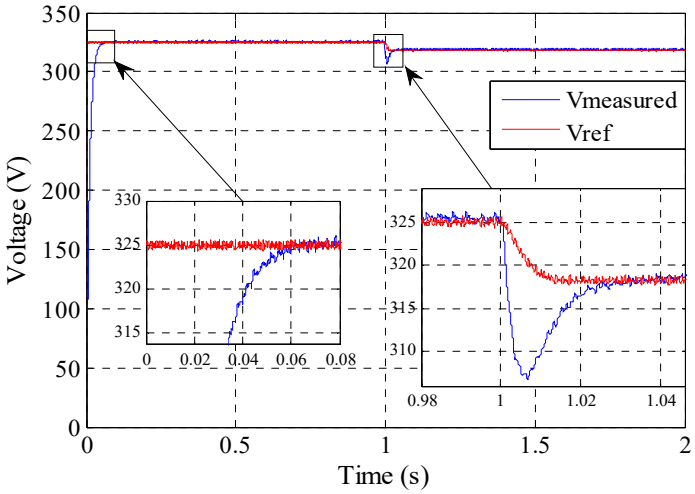


Figure 13. The voltage response of the $LQR - PI$ regulator without secondary control.

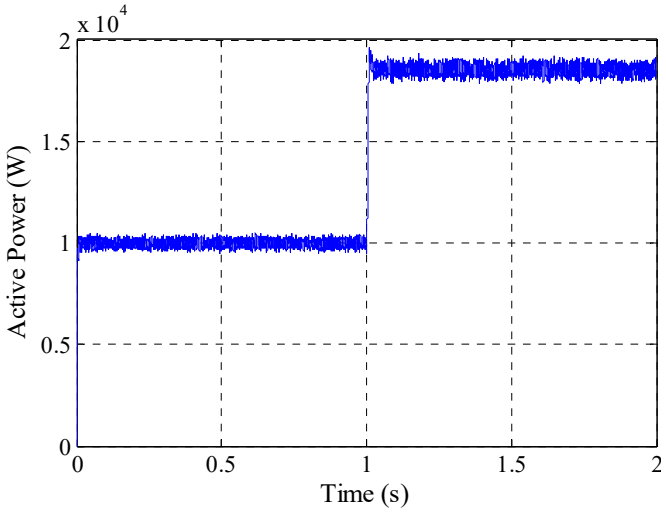


Figure 14. Active power response of the $LQR - PI$ regulator without secondary control.

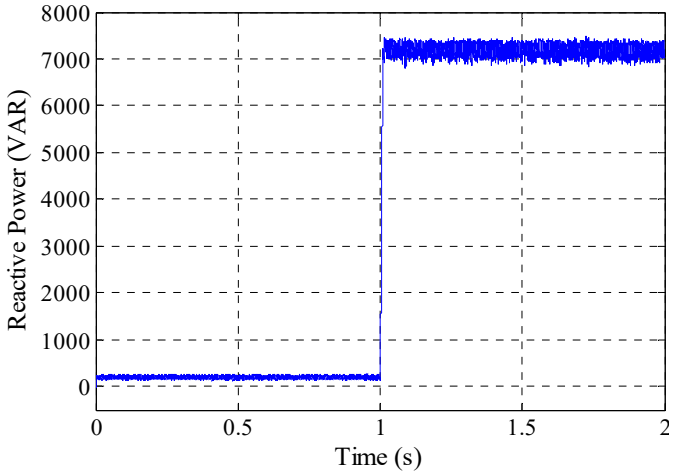


Figure 15. Reactive power response of the $LQR - PI$ regulator without secondary control.

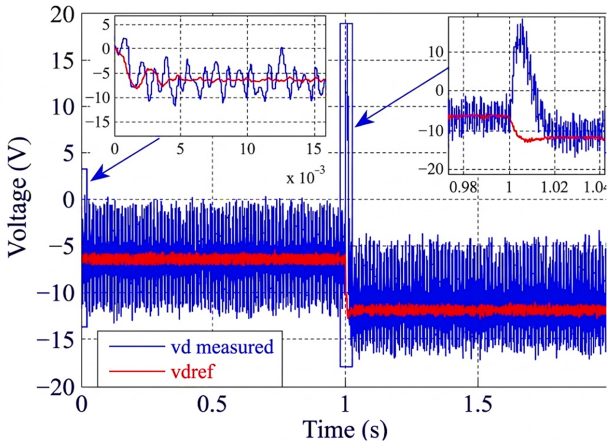


Figure 16. Voltage for the d-axis response of the $LQR - PI$ regulator without secondary control.

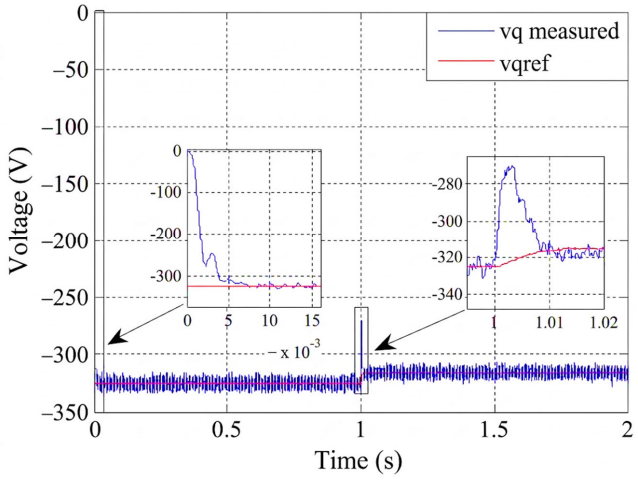


Figure 17. The voltage for the q-axis response of the $LQR - PI$ regulator without secondary control.

4.1.3. Scenario 3: Response of PI and $LQR - PI$ Regulators with Secondary Control

Figures 18–21 illustrate the system's performance when secondary control is activated in combination with both PI and $LQR - PI$ regulators. The results demonstrate that secondary control, when integrated with the fast response characteristics of the $LQR - PI$ regulator, effectively restores the output frequency and voltage to their nominal values following load disturbances. In this scenario, the frequency and voltage deviations observed

in earlier cases are rapidly corrected, confirming the successful coordination between the primary $LQR - PI$ and secondary control layers. Additionally, the Ps and Qs responses show improved stability and tracking, further validating the enhanced performance of the proposed control strategy. The comparative results highlight the advantage of using $LQR - PI$ in conjunction with secondary control, as it combines fast transient response with long-term setpoint restoration, ensuring both dynamic performance and steady-state accuracy in the DG system.

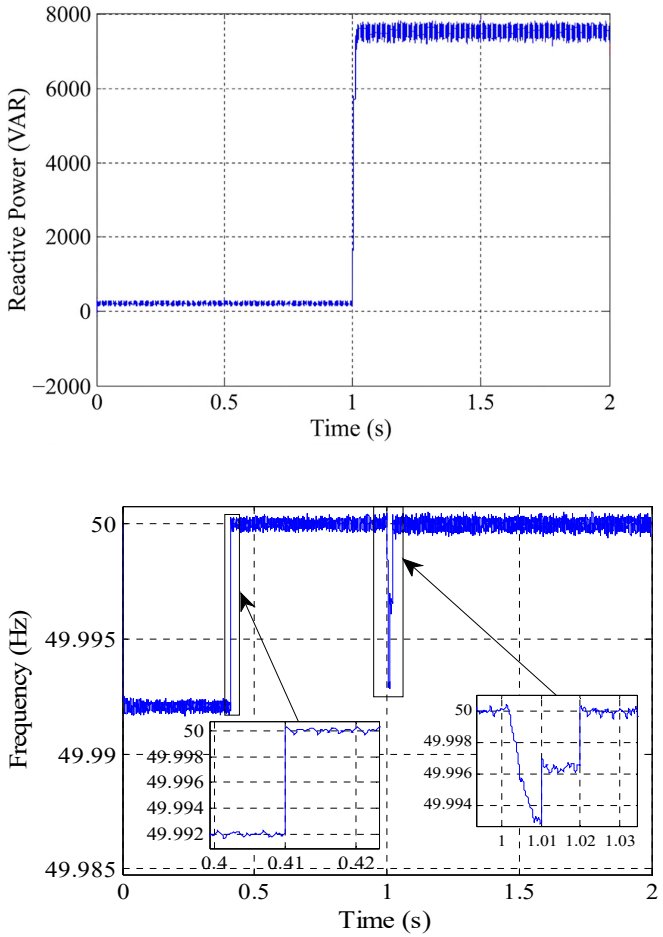


Figure 18. The frequency response of the $LQR - PI$ regulator with secondary control.

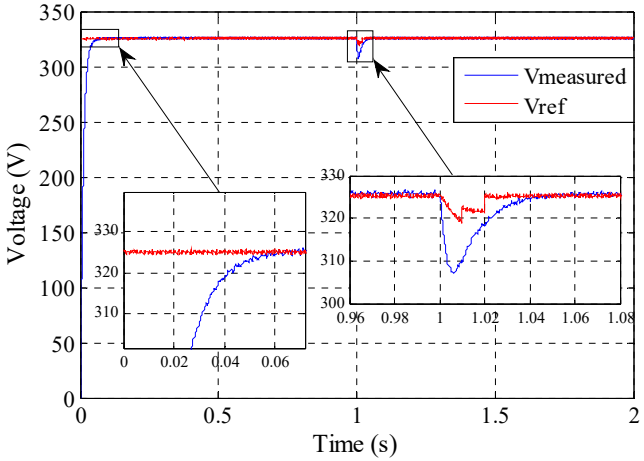


Figure 19. The voltage response of the $LQR - PI$ regulator with secondary control.

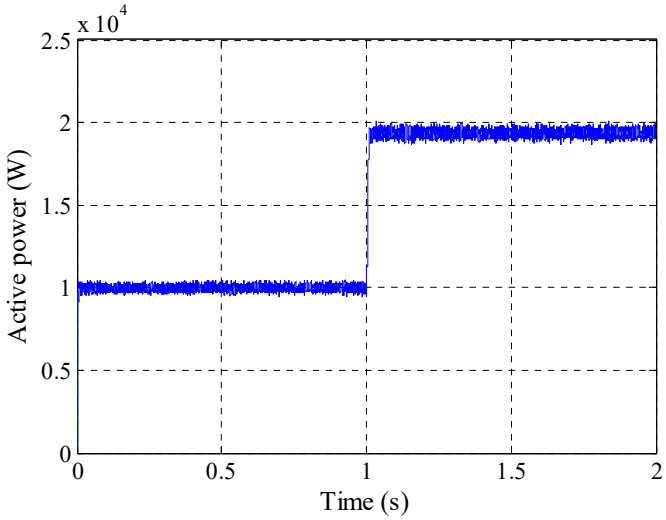


Figure 20. Active power response of the $LQR - PI$ regulator with secondary control.

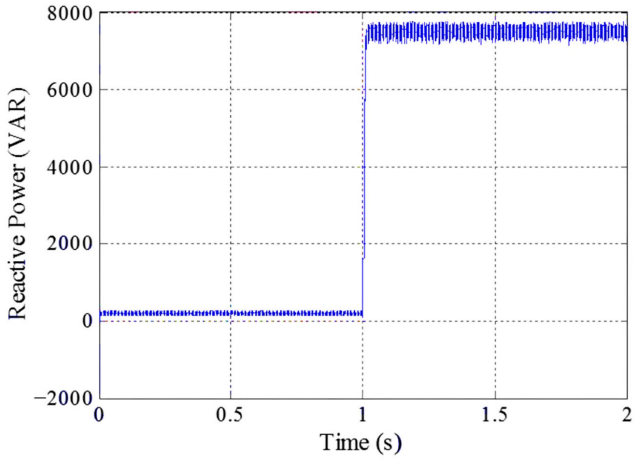


Figure 21. Reactive power response of the $LQR - PI$ regulator with secondary control.

The secondary control effectively restored the system frequency and the inverter's output voltage to their nominal values. However, this restoration was achieved with a notable delay, primarily due to the slower dynamic response of the conventional PI regulator. This delayed behavior is further emphasized in Figures 22–25, which highlight the regulator's limited ability to respond promptly to system disturbances.

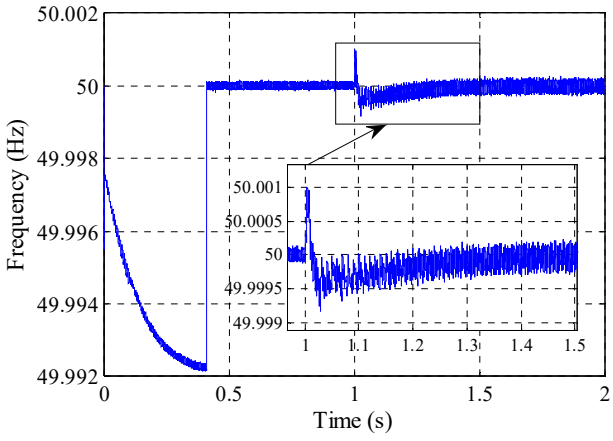


Figure 22. The frequency response of the PI controller with secondary control.

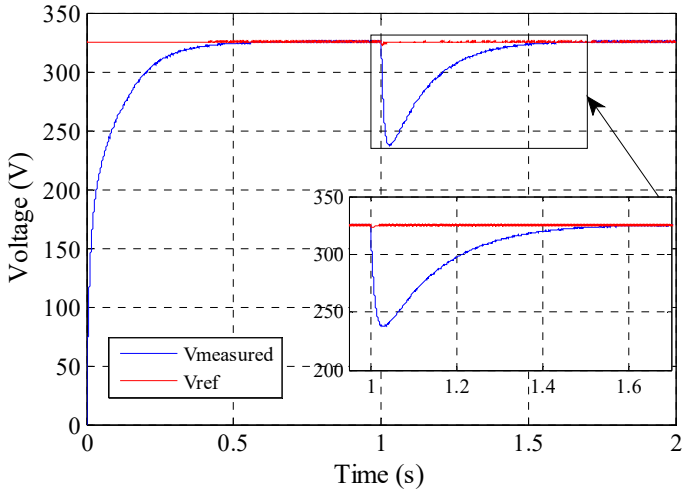


Figure 23. The voltage response of the PI controller with secondary control.

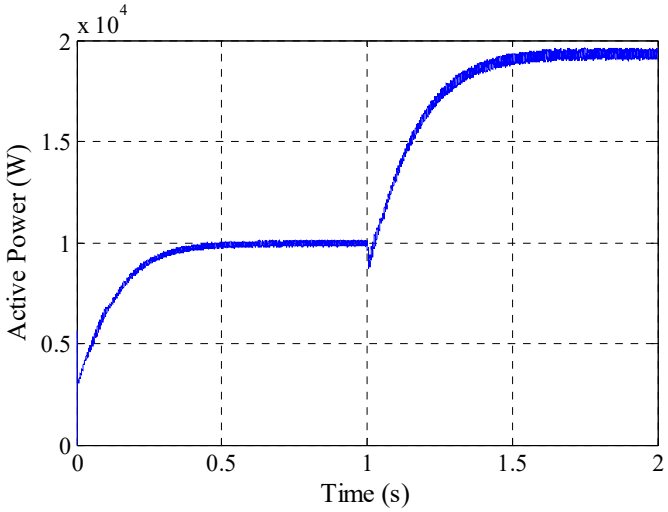


Figure 24. Active power response of the PI controller with secondary control.

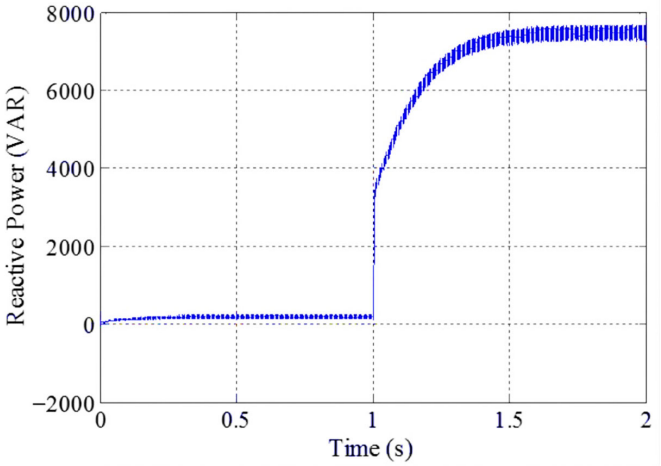


Figure 25. Reactive power response of the PI controller with secondary control.

4.2. THD Analysis Evaluation Using FFT

Figures 26–29 present the harmonic distortion analysis of the inverter output current and line-to-line voltage under the proposed LQR–PI control strategy and the conventional PI control approach. Figures 26 and 27 illustrate the current and voltage THD performance

of the proposed $LQR - PI$ controller, respectively. The THD analysis shows that the proposed $LQR - PI$ control technique reduced both voltage and current THD compared with the conventional PI control. Specifically, it achieved a current THD of 0.58% compared to 0.76% for the PI controller and a voltage THD of 1.76% compared to 1.79% for the PI controller. For the 230 V system considered in this study, IEEE 519-2022 specifies a maximum individual voltage harmonic distortion of 5% and a total voltage THD limit of 8% at the point of common coupling (PCC) [79]. The obtained voltage THD is therefore below the specified voltage distortion limit. These results confirm the good harmonic performance of the proposed $LQR - PI$ control technique and its contribution to improving the overall power quality. Table 2 presents a comparison of THD results for various published control methods. The results demonstrate that the optimal state feedback mechanism provided by the LQR regulator effectively improved the dynamic behavior of the inverter system by reducing harmonic components under both transient and steady-state operating conditions. The integration of LQR with PI regulation enabled faster compensation of load variations and improved the quality of the generated voltage and current waveforms.

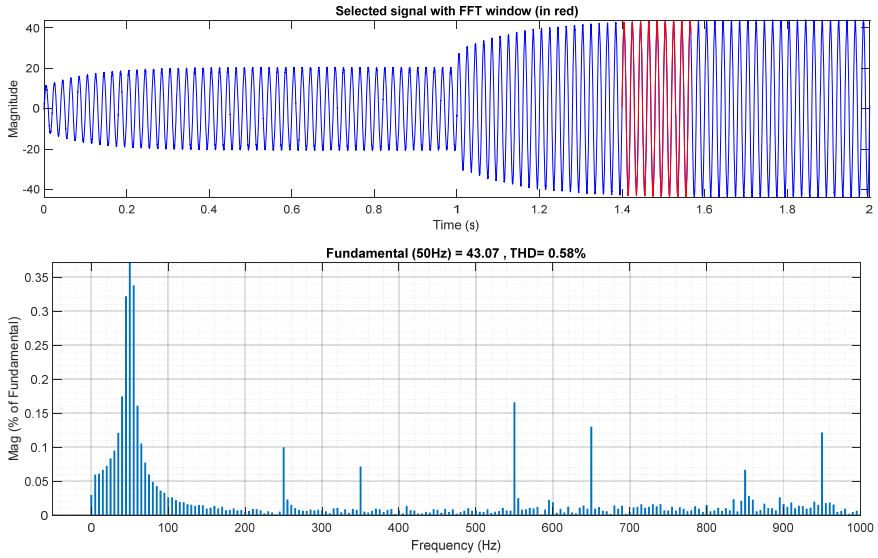


Figure 26. Analysis of current THD of $LQR - PI$ control.

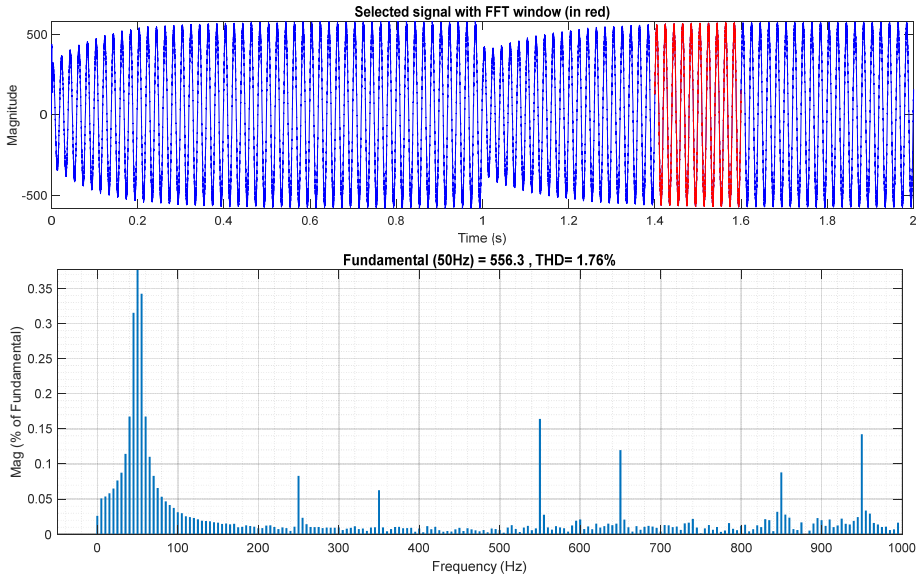


Figure 27. Analysis of voltage THD of $LQR - PI$ control.

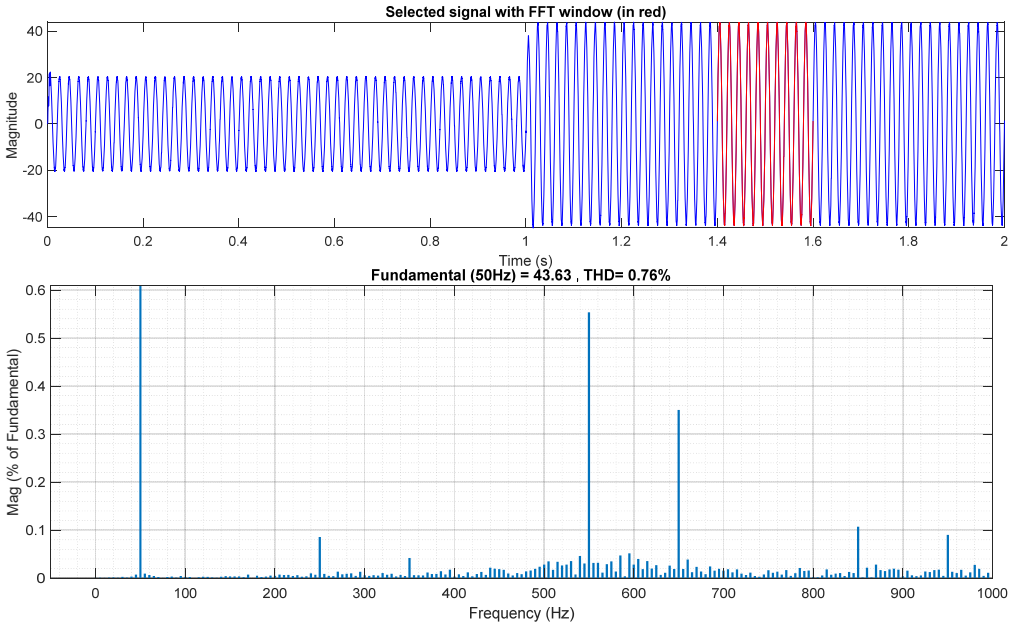


Figure 28. Analysis of current THD of PI control.

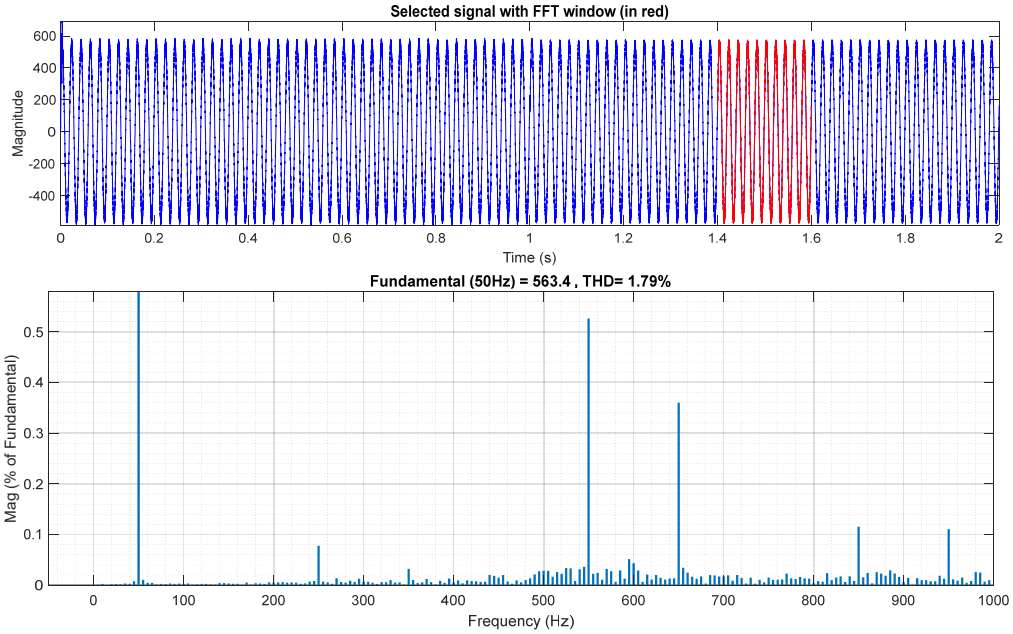


Figure 29. Analysis of voltage THD of PI control.

Comparing these results with other well-known control techniques proves that the proposed technique is efficient. For example, the simple PI method yielded very high THD values of 35.2% for current and 29.5% for voltage, which are unacceptable. Even improved versions of PI, like PI-MR with UPQC and PI-MR with M-UPQC, still had higher THD levels (e.g., PI-MR with M-UPQC showed 5.3% current THD and 4.4% voltage THD) than $LQR - PI$. Some newer techniques, like STF (49.64% ITHD, 68.51% VTHD), showed extremely poor performance, making them unsuitable for practical use. Others, such as CSA (5.56%, 8.7%), LA (5.02%, 7.1%), and AEM-SRC-SCMLI (2.19%, 14.14%), have been improved but still suffer from voltage or current distortions above the recommended value or higher than $LQR - PI$. Intelligent control techniques based on optimization, such as atomic search optimization (ASO) and ANN control, have improved THD further, from around 3.41% to 3.05% for the current. However, they still did not outperform $LQR - PI$,

particularly for voltage control, where $LQR - PI$ achieved one of the lowest voltage THD values (1.76%) ever recorded. Other advanced methods, including SCSO (3.00%, 2.00%), KFHM (2.49%, -), and MPC (8.20%, 3.20%), also reduced THD to some extent, but again not as much as $LQR - PI$. Even the very robust SMC gave a current THD of 9.60% and a voltage THD of 3.80%, with much poorer harmonic suppression. Some PWM-based control techniques such as ST-PWM (1.53%, 7.45%) and FSV-PWM (1.18%, 4.73%) gave low current distortion but suffered from voltage harmonics. In contrast, the modified PI regulator, as good as it was, still had a current distortion of 0.76% and a voltage distortion of 1.79%, slightly less than the $LQR - PI$ regulator.

Table 2. Comparison of THD results of various published control methods.

Control Techniques	Year of Application	THDi (%)	THDv (%)	References
STF Technique	2021	49.64	68.51	[38]
VOC	2021	1.64	1.60	[39]
VSM		3.60	1.71	
Droop Control		3.63	1.73	
CSA	2024	5.56	8.7	[40]
LA		5.02	7.1	
AEM-SRC-SCMLI	2024	2.19	14.14	[41]
SMC	2024	9.60	3.80	[42]
MPC		8.20	3.20	
VOC with Novel Active Damping	2020	4.56	------	[43]
ASO	2021	3.41	4	[44]
ANN Control	2024	3.05	------	[45]
SCSO	2024	3.00	2.00	[46]
KFHM Techniques	2024	2.49	------	[47]
PI-MR	2022	35.2	29.5	[48]
PI-MR with UPQC		16.2	12.1	
PI-MR With M-UPQC		5.3	4.4	
MPC-TSP	2021	2.20	5.70	[49]
ST-PWM	2022	1.53	7.45	[50]
FSV-PWM		1.18	4.73	
Modified PI	2025	0.76	1.79	-
Proposed Control		0.58	1.76	

A comparative analysis of the presented results confirms that the proposed LQR–PI control strategy achieves superior harmonic performance compared with the conventional PI controller. The reduction in voltage and current THD indicates improved PQ and more effective regulation of inverter output variables. These results demonstrate that the proposed control framework provides enhanced robustness against load disturbances while maintaining compliance with PQ requirements, making it suitable for advanced inverter-based MG applications.

5. Conclusions

This paper presents an advanced hybrid control framework for inverter-based DERs in island MGs, aimed at enhancing dynamic stability, voltage/frequency regulation, and PQ performance. The proposed strategy integrates an optimal LQR with a conventional PI controller, combined with droop control, virtual impedance, and secondary voltage/frequency restoration mechanisms. This coordinated control structure provides an effective solution for next-generation inverter-based power systems by improving disturbance rejection capability and maintaining reliable operation under dynamic loading conditions. The proposed LQR–PI controller was evaluated through MATLAB/Simulink simulations under dynamic load disturbances and compared with a conventional PI-based control strategy. The results demonstrate that the proposed approach significantly improved the inverter system's transient performance while maintaining voltage and frequency within the required IEEE operational limits ($\pm 5\%$ voltage deviation and $\pm 1.4\%$ frequency deviation). The integration of optimal state feedback enabled faster system response and improved robustness against load variations. The main findings of this study can be summarized as follows: (i) the proposed $LQR - PI$ controller reduced the frequency stabilization time by approximately 60%, decreasing the settling time from 0.5 s to 0.2 s compared with conventional PI control; (ii) the voltage recovery time was improved by approximately 50%, reducing the restoration period from 0.5 s to 0.25 s; and (iii) the proposed LQR–PI strategy reduced both voltage and current THD compared with the conventional PI control, despite the higher control energy, demonstrating improved harmonic performance and overall power quality under dynamic operating conditions. Furthermore, the incorporation of virtual impedance improved power-sharing accuracy among distributed inverters by mitigating line impedance mismatches, while the secondary control layer effectively restored voltage and frequency after disturbances. These results confirm that the proposed framework provides improved transient stability, harmonic performance, and operational reliability compared with traditional PI-based inverter control approaches. Although the proposed strategy was validated through detailed simulation studies, future research will focus on real-time experimental validation using hardware-in-the-loop (HIL) platforms and digital control implementations. In addition, future investigations will explore adaptive and intelligent control mechanisms, including machine learning-based optimization techniques, to enhance the autonomous tuning capability of inverter controllers under uncertain renewable generation, variable loading conditions, and multi-source hybrid AC/DC microgrid configurations. The proposed hybrid LQR–PI control strategy represents a promising approach for advanced inverter control in decentralized renewable energy systems, providing a practical balance between optimal dynamic performance, PQ enhancement, and implementation feasibility.

Author Contributions: D.S.: Conceptualization; methodology; software; simulation; validation; investigation; writing—original draft. D.T.: Supervision; project administration; methodology; writing—review and editing. E.A.-E.: Writing—review and editing, formal analysis, supervision, investigation M.L.: Validation; formal analysis; resources; writing—review and editing. S.A.: Data curation; visualization; investigation; writing—review and editing. R.B.: Supervision; conceptualization; resources; writing—review and editing. A.A.: Validation; methodology; writing—review and editing. M.I.M.: Writing—review and editing, formal analysis, supervision, investigation. All authors have read and agreed to the published version of the manuscript.

Funding: This research received no external funding.

Data Availability Statement: Data will be made available upon request from the corresponding author.

Conflicts of Interest: The authors declare no conflicts of interest.

Appendix A

Table A1 presents the parameters of the power stage and the controller used in this paper.

Table A1. Power stage and controller parameters.

	Parameters	VSI
Power Stage Parameters	Maximum active power rating	100 KW
	Maximum reactive power rating	20 KV
	Inverter switching frequency	20 KHz
	Nominal AC voltage	230 V
	RMS line voltage	400 V
	Nominal bus frequency	50 Hz
	DC bus voltage	800 V
	Filter inductor and the equivalent series resistance L_f and R_f	5 mH and 0.5 Ω
	Filter capacitor and the equivalent series resistance C_f and R_{cf}	10 µF and 20 Ω
	Load side line inductance and the equivalent series resistance L_l and R_l	1 mH and 65 Ω
	Inductor and resistor of virtual impedance	1 mH and 0 Ω
Controller Parameters	Droop Control	
	Proportional frequency droop P-f/Q-V	5×10^{-6}
	Proportional voltage droop P-f/Q-V	2.8750×10^{-4}
	Voltage PI control	
	Proportional voltage term K_{pv}	0.07
	Integral voltage term K_{iv}	1.225
	Current PI control	
	Proportional current term K_{pi}	34.5
	Integral current term K_{ii}	612.5

References

1. Eltohamy, M.S.; Aldawsari, M.S.; Raouf, A.; Youssef, H.; Ahmed, I.; Alsenani, T.R.; Kim, Y.-S.; Ahmed, M.M.R. Enhancing Electric Grid Flexibility for the Integration of Variable Renewable Energy: Challenges, Innovations, and Future Directions. *IEEE Access* **2026**, *14*, 23080–23109. [CrossRef]
2. Ahmad, G.; Hassan, A.; Islam, A.; Shafiullah, M.; Abido, M.A.; Al-Dhaifallah, M. Distributed Control Strategies for Microgrids: A Critical Review of Technologies and Challenges. *IEEE Access* **2025**, *13*, 60702–60719. [CrossRef]
3. Michailidis, P.; Minelli, F.; Coban, H.H.; Michailidis, I.; Kosmatopoulos, E. Reinforcement Learning for Optimizing Renewable Energy Utilization in Smart Grids: Recent Advances in Power Grids, Microgrids, and Building Energy Systems. *Infrastructures* **2026**, *11*, 240. [CrossRef]
4. Satapathy, A.S.; Mohanty, S.; Mohanty, A.; Rajamony, R.K.; Soudagar, M.E.M.; Khan, T.Y.; Kalam, M.; Ali, M.M.; Bashir, M.N. Emerging Technologies, Opportunities and Challenges for Microgrid Stability and Control. *Energy Rep.* **2024**, *11*, 3562–3580. [CrossRef]
5. Razmi, D.; Lu, T. A Literature Review of the Control Challenges of Distributed Energy Resources Based on Microgrids: Past, Present and Future. *Energies* **2022**, *15*, 4676. [CrossRef]
6. Muhtadi, A.; Pandit, D.; Nguyen, N.; Mitra, J. Distributed Energy Resources Based Microgrid: Review of Architecture, Control, and Reliability. *IEEE Trans. Ind. Appl.* **2021**, *57*, 2223–2235. [CrossRef]
7. Souza, M.E.; Henrique, T.D.M.; Rodrigues, D.B.; Guimarães, É.C.; Coelho, E.A.; Freitas, L.C. Unified Control Strategy for Islanded, Seamless Transition, and Grid-Connected Operations of Inverter-Based Distributed Generation and Microgrids. *IEEE Access* **2025**, *13*, 202253–202274. [CrossRef]

8. D'Silva, S.; Shadmand, M.; Bayhan, S.; Abu-Rub, H. Towards Grid of Microgrids: Seamless Transition Between Grid-Connected and Islanded Modes of Operation. *IEEE Open J. Ind. Electron. Soc.* **2020**, *1*, 66–81. [CrossRef]
9. Sun, L.; Sun, K.; Hou, Y.; Hu, J. Optimized Autonomous Operation Control to Maintain the Frequency, Voltage and Accurate Power Sharing for DGs in Islanded Systems. *IEEE Trans. Smart Grid* **2020**, *11*, 3885–3895. [CrossRef]
10. Nurunnabi, M.; Li, S.; Das, H.S. Advancing Grid-Forming Inverter Technology: Comprehensive PQ Capability and Performance Analysis. *IEEE Access* **2025**, *13*, 73391–73407. [CrossRef]
11. Center for Climate and Energy Solutions. Microgrids. Available online: https://www.c2es.org/content/microgrids/ (accessed on 18 June 2025).
12. Feng, W.; Jin, M.; Liu, X.; Bao, Y.; Marnay, C.; Yao, C.; Yu, J. A Review of Microgrid Development in the United States: A Decade of Progress on Policies, Demonstrations, Controls, and Software Tools. *Appl. Energy* **2018**, *228*, 1656–1668. [CrossRef]
13. Furqan, M.; Boudet, H. Nuances of Valuing Resilience from Microgrids. *Renew. Sustain. Energy Rev.* **2025**, *210*, 115236. [CrossRef]
14. Gandhi, K.; Gupta, S.K. Operational Strategies and Electricity Market Structure of Microgrid: A Critical Review. *Renew. Energy Focus* **2021**, *39*, 163–171. [CrossRef]
15. Boruah, D.; Chandel, S.S. Challenges in the Operational Performance of Six 15–19 kWp Photovoltaic Mini-Grid Power Plants in the Jharkhand State of India. *Energy Sustain. Dev.* **2023**, *73*, 326–339. [CrossRef]
16. Ainah, P.K.; Folly, K.A. Development of Micro-Grid in Sub-Saharan Africa: An Overview. *Int. Rev. Electr. Eng.* **2015**, *10*, 633. [CrossRef]
17. Ajewole, T.O.; Olabode, O.E.; Babalola, O.S.; Omoigui, M.O. Use of Experimental Test Systems in the Application of Electric Microgrid Technology Across Sub-Saharan Africa: A Review. *Sci. Afr.* **2020**, *8*, e00435. [CrossRef]
18. UnivDatos Market Insights. Europe Microgrid Market. Available online: https://univdatos.com/reports/europe-microgrid-market (accessed on 18 June 2025).
19. European Commission Directorate-General for Regional and Urban Policy. ALPGRIDS: Local Grids for Reliable Renewable Energy in the Alps. Available online: https://ec.europa.eu/regional_policy/projects/projects-database/alpgrids-local-grids-for-reliable-renewable-energy-in-the-alps_en (accessed on 11 June 2025).
20. Ember. Powering China's New Era of Green Electrification. Available online: https://ember-energy.org/latest-insights/powering-chinas-new-era-of-green-electrification/ (accessed on 22 February 2025).
21. Wei, P.; Chen, W. Microgrid in China: A Review in the Perspective of Application. *Energy Procedia* **2019**, *158*, 6601–6606. [CrossRef]
22. Singaravel, R.; Allamsetty, H.; Natarajan, S. Evolution of Microgrid, Hierarchical Architecture of Microgrid. In *Electric Vehicles and Distributed Generation-Microgrid*; River Publishers: Gistrup, Denmark, 2025; pp. 147–167.
23. Nawaz, F.; Pashajavid, E.; Fan, Y.; Batool, M. A Comprehensive Review of the State-of-the-Art of Secondary Control Strategies for Microgrids. *IEEE Access* **2023**, *11*, 102444–102459. [CrossRef]
24. Navarro-Rodríguez, Á.; García, P.; Gómez-Aleixandre, C.; Blanco, C. Cooperative Primary Control of a Hybrid AC/DC Microgrid Based on AC/DC Virtual Generators. *IEEE Trans. Energy Convers.* **2022**, *37*, 2837–2850. [CrossRef]
25. Jiang, X.; Leng, J.; Qu, S.; Gao, Z.; Zhao, W.; Meng, J. Accurate Reactive Power Sharing and Voltage-Frequency Recovery Strategy for Multiple Grid-Forming Converters Based on Consensus Algorithms. *Energy Rep.* **2026**, *15*, 109084. [CrossRef]
26. Belgacem, M.; Khatir, M.; Djehaf, M.A.; Zidi, S.A.; Bouddou, R. Implementation of DC Voltage Controllers on Enhancing the Stability of Multi-Terminal DC Grids. *Int. J. Electr. Comput. Eng.* **2021**, *11*, 1894–1904. [CrossRef]
27. Adiche, S.; Larbi, M.; Toumi, D.; Bouddou, R.; Bajaj, M.; Bouchikhi, N.; Belabbes, A.; Zaitsev, I. Advanced Control Strategy for AC Microgrids: A Hybrid ANN-Based Adaptive PI Controller with Droop Control and Virtual Impedance Technique. *Sci. Rep.* **2024**, *14*, 31057. [CrossRef] [PubMed]
28. Belgacem, M.; Khatir, M.; Djehaf, M.A.; Bouddou, R.; Benhamida, F. Analysis and Impacts of Implementing Droop Control in Multi-Terminal VSC-HVDC Under the Steady-State and Transient Stability. In Proceedings of the 2020 International Conference on Electrical and Information Technologies (ICEIT), Rabat, Morocco, 4–7 March 2020; pp. 1–6.
29. Sheykhi, N.; Salami, A.; Guerrero, J.M.; Agundis-Tinajero, G.D.; Faghihi, T. A Comprehensive Review on Telecommunication Challenges of Microgrids Secondary Control. *Int. J. Electr. Power Energy Syst.* **2022**, *140*, 108081. [CrossRef]
30. Samy, M.; Saad, N.H.; Mokhtar, M. A Lightweight Polynomial Regression Controller for Sustainable Grid-Connected DC Microgrids with Enhanced Voltage Regulation. *Sustainability* **2026**, *18*, 9320. [CrossRef]
31. Liu, X.; Zhao, T.; Deng, H.; Wang, P.; Liu, J.; Blaabjerg, F. Microgrid energy management with energy storage systems: A review. *CSEE J. Power Energy Syst.* **2022**, *9*, 483–504. [CrossRef]
32. Ullah, S.; Khan, L.; Sami, I.; Ro, J. Voltage/frequency regulation with optimal load dispatch in microgrids using SMC-based distributed cooperative control. *IEEE Access* **2022**, *10*, 64873–64889. [CrossRef]
33. Ahmad, S.; Mubarak, H.; Jhuma, U.K.; Ahmed, T.; Mekhilef, S.; Mokhlis, H. Point of common coupling voltage modulated direct power control of grid-tied photovoltaic inverter for AC microgrid application. *Int. Trans. Electr. Energy Syst.* **2023**, *2023*, 3641907. [CrossRef]
34. Safder, M.U.; Sanjari, M.J.; Hamza, A.; Garmabdari, R.; Hossain, M.A.; Lu, J. Enhancing microgrid stability and energy management: Techniques, challenges, and future directions. *Energies* **2023**, *16*, 6417. [CrossRef]

35. Somanna, B.; Gupta, S. Enhancing Reliability and Resilience in AC/DC Hybrid Microgrids: A Unified Fault Detection and Control Approach with Optimized-Tuned PI Controller for UPQC. *SN Comput. Sci.* **2025**, *6*, 247. [CrossRef]
36. Saxena, P.; Singh, N.; Pandey, A.K. Enhancing the transient performance and dynamic stability of microgrid using PI inertia injection controller. *Int. J. Electr. Power Energy Syst.* **2022**, *134*, 107334. [CrossRef]
37. Gumede, S.; Behara, K.; Sharma, G. Analytical and Optimisation-Based Strategies for Load Frequency Control in Renewable-Rich Power Systems. *Energies* **2025**, *18*, 6295. [CrossRef]
38. Aljwary, A.; Yusupov, Z.; Toirov, O.; Shokirov, R. Mitigation of load side harmonic distortion in standalone photovoltaic-based microgrid. *E3S Web Conf.* **2021**, *304*, 01010. [CrossRef]
39. Gurugubelli, V.; Ghosh, A.; Panda, A.K.; Rudra, S. Implementation and comparison of droop control, virtual synchronous machine, and virtual oscillator control for parallel inverters in standalone microgrid. *Int. Trans. Electr. Energy Syst.* **2021**, *31*, e12859. [CrossRef]
40. Gaddala, K.; Raju, P.S. Merging lion with crow search algorithm for optimal location and sizing of UPQC in distribution network. *J. Control Autom. Electr. Syst.* **2020**, *31*, 377–392. [CrossRef]
41. Meraj, S.T.; Yu, S.S.; Hasan, M.; Lipu, M.H.; Elavarasan, R.M.; Shafiullah, G.; Trinh, H. Advanced energy management scheme for fuel cell-based microgrid using self-regulated controller and switched capacitor inverter. *Int. J. Hydrogen Energy* **2024**, *90*, 1477–1494. [CrossRef]
42. Sai Sampath Kumar, P.; Suresh, P.; Lenine, D. Performance improvement of predictive voltage control for interlinking converters of integrated microgrid. *Meas. Sens.* **2024**, *33*, 101196. [CrossRef]
43. Gao, T.; Lin, Y.; Chen, D.; Xiao, L. A novel active damping control based on grid-side current feedback for LCL-filter active power filter. *Energy Rep.* **2020**, *6*, 1318–1324. [CrossRef]
44. Goud, B.S.; Rao, B.L. Power quality enhancement in grid-connected PV/wind/battery using UPQC: Atom search optimization. *J. Electr. Eng. Technol.* **2021**, *16*, 821–835. [CrossRef]
45. Rao, A.V.; Suresh Babu, G.; Satish Kumar, P. Islanded microgrid under variable load conditions for local distribution network using artificial neural network. *Smart Sci.* **2024**, *12*, 622–637. [CrossRef]
46. Shravani, C.; Rl, N.; Das, T.R. Synergetic UPQC application for power quality enhancement in microgrid distribution system: SCSO approach. *E-Prime Adv. Electr. Eng. Electron. Energy* **2024**, *10*, 100794. [CrossRef]
47. Osama abed el-Raouf, M.; A. Mageed, S.A.; Salama, M.M.; Mosaad, M.I.; AbdelHadi, H.A. Performance Enhancement of Grid-Connected Renewable Energy Systems Using UPFC. *Energies* **2023**, *16*, 4362. [CrossRef]
48. Khosravi, N.; Abdolvand, A.; Oubelaid, A.; Khan, Y.A.; Bajaj, M.; Govender, S. Improvement of power quality parameters using modulated-unified power quality conditioner and switched-inductor boost converter by optimization techniques for a hybrid AC/DC microgrid. *Sci. Rep.* **2022**, *12*, 21675. [CrossRef] [PubMed]
49. Akhtar, I.; Kirmani, S. Design and implementation of model predictive control for microgrid energy system with power quality improvement features. *Int. J. Electron.* **2021**, *108*, 1977–1998. [CrossRef]
50. Rao, S.N.V.B.; Kumar, Y.V.P.; Pradeep, D.J.; Reddy, C.P.; Flah, A.; Kraiem, H.; Al-Asad, J.F. Power quality improvement in renewable-energy-based microgrid clusters using fuzzy space vector PWM controlled inverter. *Sustainability* **2022**, *14*, 4663. [CrossRef]
51. Debdouche, N.; Zarour, L.; Benbouhenni, H.; Mehazzem, F.; Deffaf, B. Robust integral backstepping control of microgrid-connected photovoltaic system with battery energy storage through multifunctional voltage source inverter using direct power control SVM strategies. *Energy Rep.* **2023**, *10*, 565–580. [CrossRef]
52. Khallouf, K.N.; Zarour, L.; Benbouhenni, H.; Debdouche, N.; Elbarbary, Z.M.S. Adaptive fuzzy logic control for microgrid-connected hybrid photovoltaic/wind generation systems. *Energy Rep.* **2024**, *12*, 4741–4756. [CrossRef]
53. Sarra, Z.; Bouziane, M.; Bouddou, R.; Benbouhenni, H.; Mekhilef, S.; Elbarbary, Z.M.S. Intelligent control of hybrid energy storage system using NARX-RBF neural network techniques for microgrid energy management. *Energy Rep.* **2024**, *12*, 5445–5461. [CrossRef]
54. Debdouche, N.; Chebabhi, A.; Benbouhenni, H.; Hadjaidji, F.-Z.; Elbarbary, Z.M.S.; Al-Gahtani, S.F. Synergetic simplified super-twisting algorithm control for stability enhancement of PV/BESS-based DC microgrid. *Sci. Rep.* **2025**, *15*, 7392. [CrossRef] [PubMed]
55. Maroua, B.; Laid, Z.; Benbouhenni, H.; Elbarbary, Z.M.S.; Colak, I.; Alammar, M.M. Genetic algorithm type-2 fuzzy logic controller of microgrid system with a fractional-order technique. *Sci. Rep.* **2025**, *15*, 6318, Correction in *Sci. Rep.* **2025**, *15*, 14566.. [CrossRef] [PubMed]
56. Ouahabi, M.S.; Barkat, S.; Benyounes, A.; Rekioua, T.; Ihammouchen, S.; Benbouhenni, H.; Elbarbary, Z.M.S.; Alammar, M.M. Decentralized active fault tolerant control of direct current microgrids under actuator and source disturbances using proportional integral unknown input observer. *Sci. Rep.* **2025**, *15*, 14393. [CrossRef] [PubMed]
57. Chebabhi, A.; Benkhoris, M.F.; Debdouche, N.; Anwar, G.; Bizon, N.; Ihammouchen, S.; Rekiwa, T.; Benbouhenni, H. Enhanced grid current and DC voltage regulations for three-level four-leg rectifier DC microgrid under uncertainty and disturbances. *Sci. Rep.* **2025**, *15*, 23938. [CrossRef] [PubMed]

58. Maroua, B.; Laid, Z.; Benbouhenni, H.; Fateh, M.; Debdouche, N.; Colak, I. Robust type 2 fuzzy logic control microgrid-connected photovoltaic system with battery energy storage through multi-functional voltage source inverter using direct power control. *Energy Rep.* **2024**, *11*, 3117–3134. [CrossRef]
59. Alouache, B.; Helaimi, M.; Belhadj Djilali, A.; Gabbarb, H.A.; Benbouhenni, H.; Bouddou, R.; Yahdou, A.; Bizon, N. Advanced frequency control in isolated microgrids with electric vehicle aggregation: A multi-stage PID controller based on CDM technique under various operating conditions. *Heliyon* **2026**, *12*, e45136. [CrossRef]
60. Govind, D.; Suryawanshi, H.M.; Nachankar, P.; Narayana, C.L.; Singhal, A. A Modified Voltage Controller with Advanced Droop Control for Load Sharing in Standalone AC Microgrid under Different Load Conditions. *IEEE Trans. Ind. Appl.* **2023**, *59*, 5818–5831. [CrossRef]
61. Ding, M.; Tao, Z.; Hu, B.; Tan, S.; Yokoyama, R. Parallel operation strategy of inverters based on an improved adaptive droop control and equivalent input disturbance approach. *Electronics* **2024**, *13*, 486. [CrossRef]
62. Bouzid, A.M.; Sicard, P.; Abourida, S.; Paquin, J.-N. Secondary voltage and frequency restoration control of droop-controlled inverter-based microgrids. In *Proceedings of the 9th IEEE-GCC Conference and Exhibition (GCCCE)*; IEEE: Manama, Bahrain, 2017.
63. Zhong, Q.-C.; Zeng, Y. Universal droop control of inverters with different types of output impedance. *IEEE Access* **2016**, *4*, 702–712. [CrossRef]
64. Shahgholian, G.; Moradian, M.; Fathollahi, A. Droop control strategy in inverter-based microgrids: A brief review on analysis and application in islanded mode of operation. *IET Renew. Power Gener.* **2025**, *19*, e13186. [CrossRef]
65. Guerrero, J.M.; Chandorkar, M.; Lee, T.-L.; Loh, P.C. Advanced control architectures for intelligent microgrids—Part I: Decentralized and hierarchical control. *IEEE Trans. Ind. Electron.* **2013**, *60*, 1254–1262. [CrossRef]
66. Tayab, U.B.; Roslan, M.A.B.; Hwai, L.J.; Kashif, M. A review of droop control techniques for microgrid. *Renew. Sustain. Energy Rev.* **2017**, *76*, 717–727727. [CrossRef]
67. Gaonkar, D.N.; Guerrero, J.M. Improved Pf/QV and PV/Qf droop controllers for parallel distributed generation inverters in AC microgrid. *Sustain. Cities Soc.* **2018**, *41*, 421–442. [CrossRef]
68. Buraimoh, E.; Aluko, A.O.; Oni, O.E.; Davidson, I.E. Decentralized virtual impedance-conventional droop control for power sharing for inverter-based distributed energy resources of a microgrid. *Energies* **2022**, *15*, 4439. [CrossRef]
69. Eskandari, M.; Li, L. Microgrid operation improvement by adaptive virtual impedance. *IET Renew. Power Gener.* **2019**, *13*, 296–307. [CrossRef]
70. Mo, T.; Li, N.; Li, J.; Zhang, Z.; Pan, J. A droop control method based on adaptive virtual impedance for parallel control of distributed generators. In *Proceedings of the 10th International Conference on Power Electronics Systems and Applications (PESA)*; IEEE: Piscataway, NJ, USA, 2024; pp. 1–7. [CrossRef]
71. Moutevelis, D.; Roldan-Perez, J.; Jankovic, N.; Prodanovic, M. Recursive Secondary Controller for Voltage Profile Improvement Based on Primary Virtual Admittance Control. *IEEE Trans. Smart Grid* **2023**, *14*, 4296–4311. [CrossRef]
72. Aremu, M.B.; Abdel-Nasser, M.; Alyazidi, N.M.; El-Ferik, S. Disturbance Observer-Based Bio-Inspired LQR Optimization for DC Motor Speed Control. *IEEE Access* **2024**, *12*, 152418–152429. [CrossRef]
73. Bouzid, A.E.M. Élaboration d'une Méthode de Contrôle pour Améliorer la Robustesse d'un Micro Réseau Électrique. Ph.D. Thesis, Université du Québec à Trois-Rivières, Trois-Rivières, QC, Canada, 2017.
74. Dharmawan, A.; Priyambodo, T.K. Model of linear quadratic regulator (LQR) control method in hovering state of quadrotor. *J. Telecommun. Electron. Comput. Eng.* **2017**, *9*, 135–143.
75. Jaen, C.; Pou, J.; Pindado, R.; Sala, V.; Zaragoza, J. A linear-quadratic regulator with integral action applied to PWM DC–DC converters. In *Proceedings of the IECON 2006—32nd Annual Conference on IEEE Industrial Electronics Society*; IEEE: Paris, France, 2006.
76. Valencia-Rivera, G.H.; Merchan-Villalba, L.R.; Tapia-Tinoco, G.; Lozano-Garcia, J.M.; Avina-Cervantes, J.G. Hybrid LQR–PI control for microgrids under unbalanced linear and nonlinear loads. *Mathematics* **2020**, *8*, 1096. [CrossRef]
77. Kedjar, B.; Al-Haddad, K. LQR with integral action to enhance dynamic performance of three-phase three-wire shunt active filter. In *Proceedings of the IEEE Power Electronics Specialists Conference (PESC)*; IEEE: Orlando, FL, USA, 2007.
78. Keshtkar, H.; Mohammadi, F.D.; Ghorbani, J.; Solanki, J.; Feliachi, A. Proposing an improved optimal LQR controller for frequency regulation of a smart microgrid in case of cyber intrusions. In *Proceedings of the 27th Canadian Conference on Electrical and Computer Engineering (CCECE)*; IEEE: Toronto, ON, Canada, 2014.
79. Farou, M.; Djellad, A.; Chiheb, S.; Lalaymia, H.; Logerais, P.O.; Khouzam, A.; Abdou Tankari, M. Impact of Photovoltaic Aging on Power Quality: THD-Based Evaluation with Respect to the IEEE 519-2022 Standard. *J. Comput. Electron.* **2026**, *25*, 197. [CrossRef]

Disclaimer/Publisher's Note: The statements, opinions and data contained in all publications are solely those of the individual author(s) and contributor(s) and not of MDPI and/or the editor(s). MDPI and/or the editor(s) disclaim responsibility for any injury to people or property resulting from any ideas, methods, instructions or products referred to in the content.